Climate-driven fluxes of organic-bound uranium to an alpine lake overthe Holocene

Pierre Lefebvre, Pierre Sabatier, Arnaud Mangeret, Alkiviadis Gourgiotis, Pierre Le Pape, Anne-Lise Develle, Pascale Louvat, Olivier Diez, Jean-Louis Reyss, Jérôme Gaillardet, et al.

Climate-driven fluxes of organic-bound uranium to an alpine lake over the Holocene

Pierre Lefebvre*[,a], Pierre Sabatier[b], Arnaud Mangeret[c], Alkiviadis Gourgiotis[c], Pierre Le Pape[a], Anne-Lise Develle[b], Pascale Louvat[d], Olivier Diez[c], Jean-Louis Reyss[b], Jérôme Gaillardet[d], Charlotte Cazala[c], Guillaume Morin[a]

a. *Institut de Minéralogie, de Physique des Matériaux et de Cosmochimie (IMPMC), UMR 7590 Sorbonne Université-CNRS-MNHN-IRD, Paris, France*

b. *Université Grenoble Alpes-Université Savoie Mont Blanc-CNRS-EDYTEM, UMR 5204, Le Bourget-Du-Lac, France*

c. *Institut de Radioprotection et de Sûreté Nucléaire (IRSN), PSE-ENV SEDRE, Fontenay-aux-Roses, France*

d. *Université de Paris-Institut de Physique du Globe de Paris-CNRS, UMR 7154, Paris, France*

*Corresponding author: Pierre Lefebvre, pierre.lefebvre@sorbonne-universite.fr

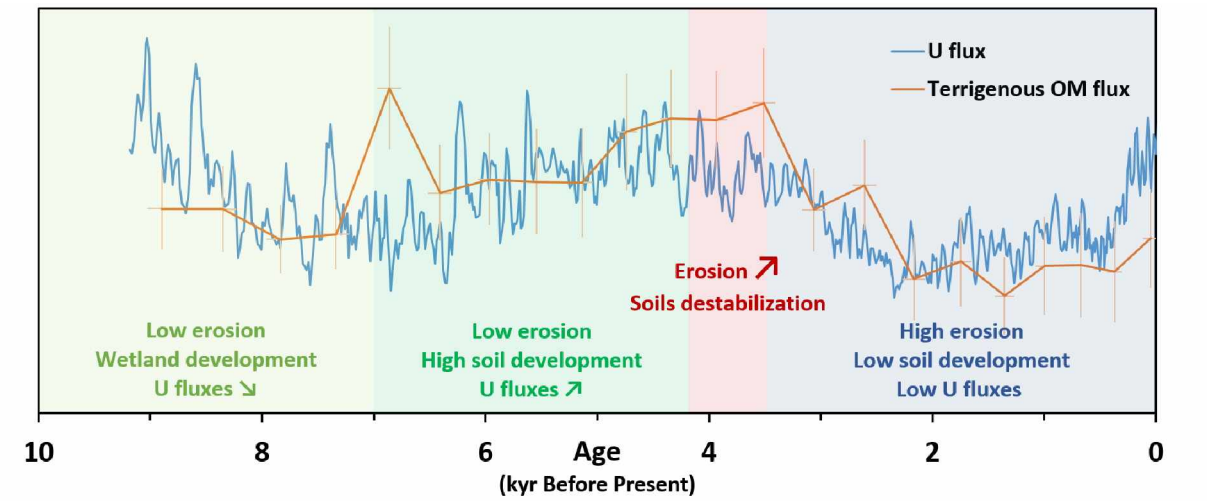

HIGHLIGHTS

1. Weathering and erosion dynamics show major changes at 4.2 kyr BP
2. Terrigenous vs. autochthonous OM inputs are driven by Holocene climatic variations
3. U binding to terrigenous organic matter controlled U sedimentation over 9.2 kyr
4. Lake bottom water oxygenation did not influence U fluxes to the sediments

ABSTRACT

Uranium (U) isotopic signatures and concentration in sediments are widely used as paleo-redox proxies, as the behavior of U is often controlled by bottom water oxygenation. Here, we investigated the processes controlling U accumulation in the sediments of Lake Nègre (Mediterranean Alps, South-East France) over the past 9200 years. Exceptionally high natural U concentrations (350-1250 $\mu g.g^{-1}$) allowed the measurement of U along with other elements by high-resolution X-Ray Fluorescence core-scanning. Weathering and erosion proxies (Ti content, Zr/Al and K/Ti ratios) indicate that sedimentary inputs were controlled by Holocene climatic variations. After a period of low erosion during the Holocene Climatic Optimum, a major regime shift was recorded at 4.2 kyr BP when terrigenous fluxes consistently increased until present with high sensitivity to centennial-scale climatic events. Sedimentary organic matter (OM) inputs were dominated by terrigenous OM from the catchment soils until 2.4 kyr BP, as attested by carbon to nitrogen (C/N) and bromine to organic carbon (Br/TOC) ratios. From 2.4 kyr BP to present, lake primary production and soils equally contributed to sedimentary OM. Uranium fluxes to the sediments were well correlated to terrigenous OM fluxes from 7 kyr BP to present, showing that U supply to the lake was controlled by U scavenging in the soils of the watershed followed by transport of U bound to detrital organic particles. Higher U/OM ratios before 7 kyr BP likely reflect the development of the upstream wetland. The fluctuations of U sedimentary inputs appear to be independent of bottom water oxygenation, as estimated from constant Fe/Mn ratios and $\delta^{238}U$ isotopic signatures, and rather controlled by the production, erosion and sedimentation of terrigenous OM. This finding confirms that the use of U (and potentially other metals with high affinity to OM) concentrations alone should be used with caution for paleo-redox reconstructions.

KEYWORDS

Lake watershed; XRF core-scanning; Terrigenous fluxes; Organic matter; Uranium cycle.

1 INTRODUCTION

Uranium (U) is a redox-sensitive element, very soluble in oxic conditions and poorly soluble when reduced (Langmuir, 1978; Maher et al., 2013), which accumulation and isotopic composition in sediments have been widely used in paleo-redox studies to reconstruct past changes in bottom ocean water oxygenation (e.g., Lau et al., 2019; Tribovillard et al., 2006). In comparison to marine settings, the uranium content of lake sediments is less documented and records more local variations in water oxygenation or U inputs from lake watersheds. Hence, most studies on lacustrine systems have focused on present-day processes of U accumulation at the sediment-water interface in pristine (Chappaz et al., 2010; Och et al., 2016) and U mining-impacted lakes (Dang et al., 2018; Stetten et al., 2018; Wang et al., 2019). Only a few studies have investigated the U distribution in lake sediments over long time scales as a tracer of paleo-environmental conditions (Edgington et al., 1996; Goldberg et al., 2010; Whitlock et al., 2012; Yang et al., 2015). U inputs to lakes could be related to past climate variations, as shown for Lake Baikal with higher U fluxes during interglacial than glacial periods (Edgington et al., 1996; Goldberg et al., 2010). Fluctuations in U inputs to the oxic waters of this lake were attributed to regional-scale hydrological variations that impacted the contributions of various U supplying rivers. The various possible mechanisms of U transport and sedimentation in lakes and their response to climatic forcing remains however to be clarified. They may indeed include dissolved or particulate transport/sedimentation, as well uranium trapping via its reduction in the water column or at the sediment-water interface (Anderson et al., 1989; Barnes and Cochran, 1990; Chappaz et al., 2010; McManus et al., 2005). To this end, the Lake Nègre catchment (Mediterranean Alps, South-East France) was chosen as case study since the lake sediments were previously shown to naturally contain exceptionally high U concentrations (Lefebvre et al., 2021).

Climatic variations (hydrology, temperature) have a direct impact on sedimentary inputs into lakes (Arnaud et al., 2016), especially in mountainous areas that are particularly sensitive to environmental changes (Beniston, 2006). As they drain small watersheds with usually quite simple geologic settings, high-altitude lakes are able to directly and specifically record climatic impacts on elemental inputs, which result in fluctuations between detrital/terrigenous and dissolved/authigenic elemental fluxes (Brisset et al., 2013; Giguet-Covex et al., 2011; Wilhelm et al., 2013). In particular, climate controls the relative intensity of physical and chemical erosion (Arnaud et al., 2012). This physicochemical effect is further complemented by the effect of temperature (T) on the development of land vegetation and lacustrine primary productivity, the latter being also constrained by nutrient availability. In addition, vegetation has an ambivalent impact on erosion as plant root development both facilitates soil weathering and chemical erosion through extension of erodible surfaces and secretion of acidic substances, and limits soil physical

erosion through soil stabilization (e.g., Bajard et al., 2017a, 2017b). The development of human activities (agriculture and pastoralism often coupled to deforestation) in accessible mountainous areas induced increasing soil erosion especially in the past two millennia, until exceeding the soil formation rate (Bajard et al., 2017a, 2017b; Brisset et al., 2013, 2017; Giguet-Covex et al., 2014).

The evolution of temperatures in the Alpine region during the Holocene can be inferred from reconstructed patterns obtained from chironomid records (Heiri et al., 2015; Samartin et al., 2017) and speleothems fluid inclusions in the Central Alps (Affolter et al., 2019) among others. Briefly, after a rapid T increase (> +5 °C) at the end of the Younger Dryas, the beginning of the Holocene (~11.5 kyr BP) was marked by a progressive warming until 9.6 to 9 kyr BP, followed by stable T during the Holocene Thermal Maximum until 6.4 to 4 kyr BP, interrupted by the 8.2 kyr BP cold event. Since 4 kyr BP under the Neoglacial period, temperatures have continuously and slowly decreased until the 20th century, influenced by temporary cold events with variable regional significance (Affolter et al., 2019; Bini et al., 2019; Martrat et al., 2014). The last 2000 years are better documented over the Northern Hemisphere, with cold periods during the so-called "Dark Ages" (1400-1100 cal BP) and especially the Little Ice Age (700-100 cal BP) and warmer periods during the Roman era and the Middle Ages (e.g., Affolter et al., 2019). Absolute T variations in the Northern Hemisphere are still debated (e.g., Marsicek et al., 2018) but consistent relative climatic variations are widely reported.

The evolution of rainfall intensity over time was inferred from occurrences of flood deposits in sediments from several alpine lakes and was thus quantified by the evolution of the flood frequency and intensity (Brisset et al., 2017; Sabatier et al., 2017; Wilhelm et al., 2012; Wirth et al., 2013). The general pattern of flood activities in the Southern Alps over the Holocene shows relatively rare extreme rainfall events until shortly before 4 kyr BP, followed by a sharp increase to higher flood frequencies, with variations following short-term climatic variations (Sabatier et al., 2017; Wirth et al., 2013). This global evolution is mainly attributed to the orbital-driven decrease in summer insolation during the Neoglacial (after ~ 4.2 kyr BP) leading to higher rainfall events (Magny et al., 2013; Vanniere et al., 2013).

Another major impact of climate changes on mountainous environments is the glacial activity that has a large impact on the production and export of fresh mineral surfaces. In the Mediterranean Alps, the last deglaciation occurred rapidly between 14,500 and 13,000 years cal BP (calibrated age Before Present, i.e., before AD 1950) during the Lateglacial Interstadial (Brisset et al., 2015, 2014) with the last influence of glaciers registered 11,000 years ago (Brisset et al., 2015). Major glacier retreats at the beginning of the Holocene allowed the formation of high-altitude lakes in the Alps, such as Lake Nègre (2354 m above sea level). On the

scale of the Alps, global glacier advances are described after 4.2 kyr BP, corresponding to the onset of the Neoglacial period (Le Roy et al., 2017, 2015).

Owing to its small catchment area and negligible anthropic activities, Lake Nègre offers the opportunity to study direct effects of climatic variations in the Mediterranean Alps on U fluxes to the sediments. In particular, its low sedimentation rate (Lefebvre et al., 2021) reflects its low sensitivity to physical erosion events (Arnaud et al., 2016), hence allowing to decipher the specific impact of chemical erosion and of the dynamics of land vegetation and lake productivity on U inputs. Exceptionally high U concentrations in Lake Nègre sediments enable the use of X-Ray Fluorescence (XRF) core-scanning to measure high-resolution (1-mm steps) sedimentary U profiles, together with other elements. In our previous study (Lefebvre et al., 2021), we investigated the solid-state speciation of U using X-ray absorption spectroscopy on a sediment core from Lake Nègre dating back to 3300 years BP and found that U initially deposits as non-crystalline organic-bound U before transforming to U-Si polymers through diagenetic aging. As U is thus thought to be deposited after binding on lake biomass or terrigenous organic matter (OM), variations in U sedimentary content are expected to be constrained both by (i) U inputs from the watershed to the lake water, and by (ii) the relative development of soil vegetation and lacustrine biomass.

In this multi-proxy study, we first investigated the responses to climatic variations of physical and chemical erosion processes, as well as inputs from different organic matter sources over the Holocene, as recorded in Lake Nègre sediments. The fluctuations of U inputs to the sediments are then described and interpreted in the light of the reconstructed lake paleo-environmental history.

2 MATERIALS AND METHODS

2.1 Study site

As Lake Nègre was previously described to investigate U mineralogical transformations in sediments over 3300 years, a full description of the study site is provided in the main text and SI appendix of Lefebvre *et al.* (2021). Briefly, Lake Nègre is located in a remote, high-altitude glacier-carved watershed, at the border between France and Italy in the Mercantour-Argentera Massif, ~50 km north of the Mediterranean Sea (Figure 1). This small watershed is essentially granitic and partially covered by scree and scarce alpine meadows, with rare occurrences of pine trees (Figure 1c). The bottom of the 28-m deep, stratified lake water column was shown to be suboxic at the time of sampling in September 2018.

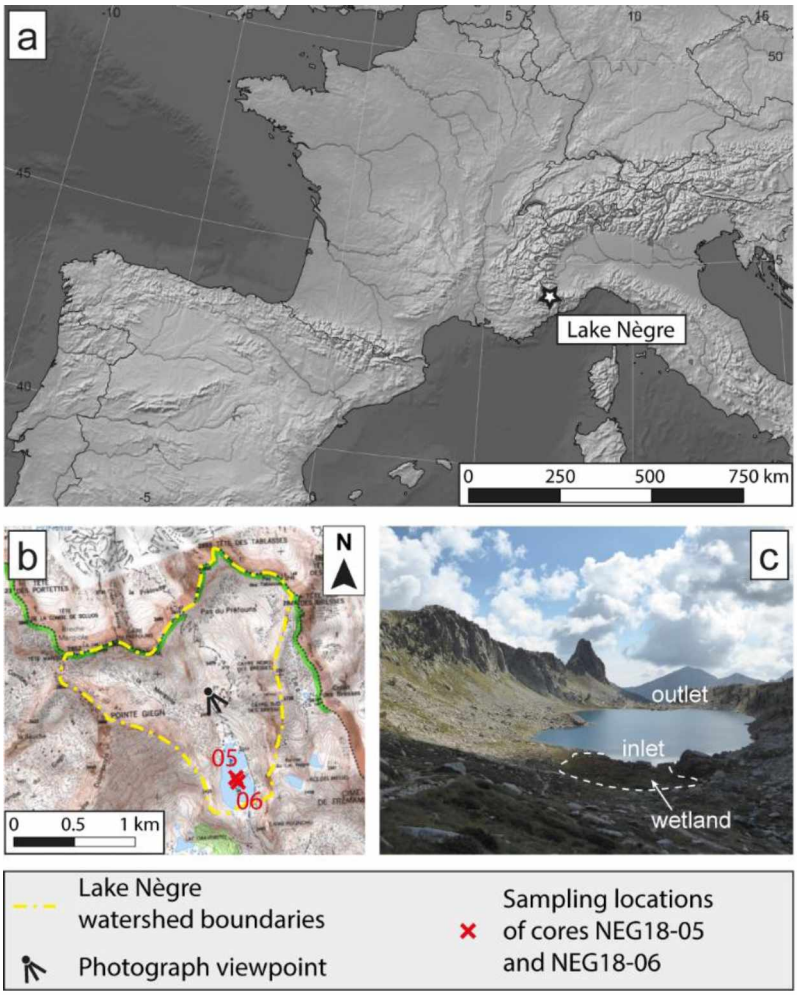

Figure 1 – Lake Nègre location and core sampling locations. *(a) Location of Lake Nègre in the Mercantour-Argentera massif, South-East France. (b) Topographic map of the Lake Nègre watershed; the watershed is delimited by a yellow dashed line, sampling locations of cores NEG18-05 and NEG18-06 are indicated by red crosses; map from BRGM (http://infoterre.brgm.fr), updated 02/11/2020. (c) Photograph of Lake Nègre, which viewpoint is indicated in (b), showing positions of the lake inlet and outlet and of the wetland right upstream of the lake, delimited by a white dashed line.*

2.2 Sampling and lithology

A series of sediment cores was sampled in September 2018 at the deepest point of Lake Nègre using a hammer-equipped Uwitec gravity corer (63 mm internal diameter). This study focuses on cores NEG18-05 (187.5 cm long, sampled at N 44° 9.49926'; E 7°14.1516') and NEG18-06 (216 cm long, sampled 20 m southward at N 44° 9.48966'; E 7°14.1576'), taken in addition to cores NEG18-04 and NEG18-07 that were specifically stored in anoxic conditions for U speciation analysis and described in Lefebvre *et al.* (2021). Both cores studied here (NEG18-05 and 06) were cut in two halves in the open air; one half was preserved for sedimentological description and XRF core-scanning, and 1 cm slices were sampled on the other half for chemical analysis. Most analyses were performed on core NEG18-06; the data presented in this article consequently refer to this core, unless stated otherwise.

As described previously (Lefebvre et al., 2021), the cores consist of three main sedimentary units. Bottom sediments (Unit B) are homogeneous and typical of brown, silty gyttja deposits widely observed in high elevation Alpine lakes following the last deglaciation (Brisset et al., 2015). Two series of seismic shots in the northern part of the lake in 1958 and 1966, performed in an attempt to determine the Moho depth below the Alps (Perrier, 1980), caused slope destabilization of the sediments, leading to the accumulation of thick mass wasted deposits (denoted as Unit S) above the pristine Unit B. The top unit (Unit T) corresponds to the last ~50 years of regular sedimentation and is composed of uncompacted clayey-silty sediments. This study focuses on pristine sediments from Unit B, deposited until the mid-twentieth century.

2.3 Geochronology

Radiocarbon dating of 16 and 3 terrestrial plant macro-remains was performed by accelerator mass spectrometry at the Poznan Radiocarbon Laboratory (Poland) along cores NEG18-06 and NEG18-05 respectively in order to build an age-depth model using the *R* software-package "clam" (*R* version 3.6.2, (R Core Team, 2019))(Blaauw, 2010) with the IntCal20 calibration curve (Reimer et al., 2020) and smooth spline interpolation (degree of smoothing of 0.4 and 0.2 for cores NEG18-06 and NEG18-05 respectively). For the age-depth model of core NEG18-05, we used two additional ^{14}C dates from core NEG18-06 thanks to core correlation based on XRF core-scanner data (Figure SI-1). The latter was complicated by accidental drying of the half core before XRF measurements, leading to several fractures that were artificially corrected (see SI text and Figure SI-2) to obtain a continuous profile, albeit with higher uncertainties.

2.4 Chemical characterization

The elemental composition of core NEG18-06 was investigated at high resolution (1 mm steps) with an Avaatech XRF core-scanner at EDYTEM laboratory. Because of its poor conservation, core NEG18-05 was analyzed every 5 mm. Light elements were measured with tube settings at 10 kV and 0.175 mA for 15 s, and heavy elements (including U) at 30 kV and 0.245 mA for 35 s. On core NEG18-06, the data noise was reduced with 3-point moving averages. Uncertainties (2 relative standard deviations – RSD) were calculated from 4-point replicates measured every 4 cm. In order to account for potential matrix effects, element ratios are expressed as logarithms (ln) of XRF counts ratios that are linearly related to the log ratios of corresponding absolute concentrations (Weltje and Tjallingii, 2008). Major, minor (Al, Ca, Fe, Na, K, Mg, Mn, P, Ti) and trace elements (U and Th) concentrations were measured by Inductively Coupled Plasma Atomic Emission and Mass Spectrometry (ICP-AES and ICP-MS) respectively at the LUTECE laboratory (IRSN), following acid digestion according to protocols detailed in Lefebvre *et al.* (2021). Silica and other major elements were determined on four samples at the Service d'Analyse des Roches et Minéraux (SARM-CRPG, Nancy, France) by optical emission spectrometry (ICP-OES) after $LiBO_2$ alkali fusion. Calibration of U and Ti XRF counts was performed with 13 sediment samples using concentrations measured by ICP-MS, with respective correlation coefficients (R^2) of 0.95 and 0.87 and *p*-values < 10^{-5} (Figure SI-3).

Organic matter characterization (total C and N concentrations, $\delta^{13}C$ and $\delta^{15}N$) was performed by the Pôle Isotopie-Chimie (UMR SILVA) of INRAE (Champenoux, France) with a Vario Isotope Elemental Analyser – Isotope Ratio Mass Spectrometer (EA-IRMS). Additional organic and inorganic carbon contents were measured with a Vario TOC Elementar carbon analyzer at LUTECE following procedures described in Stetten *et al.* (2018). No inorganic carbon could be detected, which is consistent with the absence of carbonate rocks in the Lake Nègre watershed, implying that total C is equivalent to total organic carbon (TOC).

Because of the differential solubility of U (highly soluble) and Th (insoluble) in oxic environments (Missiaen et al., 2018; Nuttin et al., 2013; Yu et al., 1999), detrital U fractions ($U_{detrital}$, in % of the total U pool) could be determined from the U/Th ratios of samples and background rocks as detailed in Lefebvre *et al.* (2021), following Equation 1:

$$U_{detrital}\,[\%] = \frac{\left(U/Th\right)_{rocks}}{\left(U/Th\right)_{sample}} \times 100 \qquad (1)$$

Radio-elements (^{238}U (from ^{234}Th), ^{230}Th, ^{228}Th, ^{228}Ra, ^{226}Ra, ^{210}Pb, ^{137}Cs, ^{40}K) were measured on core NEG18-05 by gamma spectrometry at IRSN using a HP Ge detector (EGPC 20,

Intertech) according to the protocol described in Mangeret *et al.* (2018) and a well-type high-purity/low-noise Ge ORTEC GWL Series detector following Reyss *et al.* (1995). ^{238}U activities measured by gamma spectrometry (in Bq/kg) were converted to U concentrations (in µg/g) using the ^{238}U mass activity (12.44 kBq/g).

The sediment dry bulk density (DBD) was determined at 27 depths in Unit B of core NEG18-06 by determining the dry weight of a known volume. Relative uncertainties were arbitrarily set at 10 %. The ratio of Incoherent (Compton) over Coherent (Rayleigh) scattered intensities (Inc/Coh) obtained from XRF scanning (Figure SI-4), which is a rough proxy of sediment texture (density, porosity, water content), has been shown to correlate with organic matter content (TOC, loss on ignition) in some sediments (Chawchai et al., 2016; Liu et al., 2013; Sáez et al., 2009; Woodward and Gadd, 2019) but not well enough in organic-rich gyttja sediments (Chawchai et al., 2016) such as those of Lake Nègre. Here, we found the Inc/coh ratio to be satisfyingly correlated to DBD (r^2 = 0.75, $p < 10^{-5}$; Figure SI-5), probably thanks to the homogeneity of Unit B sediments. A high-resolution (1-mm step) DBD profile was reconstructed by linear regression using the relationship between DBD and the Inc/Coh ratio, with an average propagated uncertainty of 14 % (Figure 2). The reconstructed profile is in good agreement with measured DBDs, except at the bottom of the core (210-216 cm) where a little discrepancy is noted but lies within uncertainties.

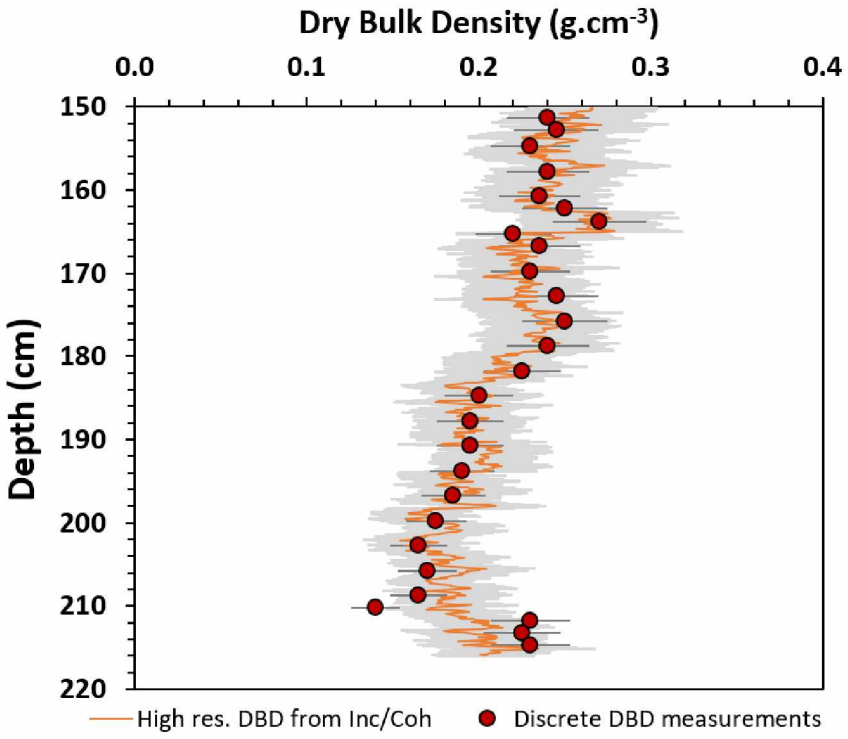

Figure 2 – Sediment dry bulk density (DBD) of core NEG18-06. *Discrete measurements (red circles) and reconstructed high-resolution DBD profile (orange line) inferred from the ratio of XRF Incoherent/Coherent scattered intensities. Error bars and grey shading represent 2SD uncertainties.*

In order to take into account (i) the effects of sediment compaction and (ii) the variations in sediment accumulation rates, we calculated the flux or mass accumulation rate F_X (in $g.m^{-2}.yr^{-1}$) of element *X* following Equation 2:

$$F_X = [X] \times \tau_{acc} \times DBD \qquad (2)$$

Where [X] is the concentration of element X in the dry solid phase of the sediment (in weight % (wt%) or µg/g), τ_{acc} is the sediment accumulation rate (in $mm.yr^{-1}$) inferred from the age-depth model and DBD is the dry bulk density of the sediment (in $g.cm^{-3}$), reconstructed *via* linear regression. For fluxes calculations, uncertainties on accumulation rates were estimated at 5 %.

2.5 Isotopic measurements

In order to correct from instrumental and analytical mass biases, samples from core NEG18-06 were double-spiked with IRMM-3636a standard with a spike/sample ratio ($^{236}U/^{235}U$) of ≈ 2-3, right after sample digestion. Following procedures detailed in Lefebvre *et al.* (2021), U was then separated from other dissolved elements using column chromatography with UTEVA resin (Eichrom Technologies, LLC). Isotopic ratios $^{234}U/^{238}U$ and $^{238}U/^{235}U$ were measured on the ThermoScientific Neptune Multi-Collector (MC) IPC-MS of the PARI platform (IPGP) with 10^{11}-ohm amplifiers for ^{235}U and ^{238}U and a 10^{13}-ohm amplifier for ^{234}U. ($^{234}U/^{238}U$) activity ratios were calculated by multiplying isotopic ratios with the ratio of the respective radioactive decay constants. The $^{238}U/^{235}U$ ratios of the samples are presented in the delta-notation ($\delta^{238}U$, in ‰) following Equation 3:

$$\delta^{238}U = \left(\frac{\left(^{238}U/^{235}U\right)_{sample}}{\left(^{238}U/^{235}U\right)_{IRMM-184}} - 1 \right) \times 1000 \qquad (3)$$

The bracketing standard IRMM-184 was used for the delta-notion calculation and in order to refer our data to the internationally recognized δ-zero standard CRM-145/CRM-112a (Andersen et al., 2017), all $\delta^{238}U$ data were corrected with an offset of -1.10 ‰ (IRMM, 2005; NBL, 2010). Uncertainties were calculated as two standard deviations (2SD) of all 3-5 replicates per sample. Three standards (BCR-2, AGV-2, HU-1) were measured along with the samples in order to control the method accuracy, and correspond to previously published values (see Lefebvre et al., 2021). Procedural blanks were found to be negligible in U contents (< 0.2 ng) compared to the U amounts processed for sample isotopic analyses (> 3000 ng).

3 RESULTS AND DISCUSSION

3.1 Geochronology

The calibrated radiocarbon dates obtained with the IntCal20 calibration curve are displayed in Table 1. Six dates showing age inversions due to the large mass wasted deposit (Unit S) were rejected, as well as one outlier date in Unit B (166.3 cm) which was obviously too old and probably reworked from the watershed (Table 1). The age-depth model of core NEG18-06 is shown in Figure 3a. The model provides a very low sedimentation rate that increased over time from 0.06 mm/yr to 0.11 mm/yr with smooth variations (Figure 3b). The deeper radiocarbon age measured at 212.5 cm was determined to be 8700 ± 110 cal BP. By extension of the age-depth model, the bottom of the core (216 cm depth) was dated at ~ 9184 cal BP. The age of the most recent Unit B sediments actually corresponds to the period of seismic shots in the second half of the 20th century. The mass wasted deposit seemingly did not significantly erode surface sediments as peak lead (Pb) accumulation corresponding to modern emission (Renberg et al., 2001; Elbaz-Poulichet et al., 2020) is still present (Figure SI-1).

Table 1 – Radiocarbon datation of core NEG18-06. *^{14}C ages (years BP) and associated ranges of calibrated ^{14}C ages (cal BP) thanks to the IntCal20 calibration curve on cores NEG18-06 and NEG18-05. Calibrated age ranges correspond to the most probable age intervals. Rejected ages are indicated in italic grey. The sample age at 48.5 cm is expressed as percent modern carbon (pMC), indicating a modern age posterior to 1950 AD. Nine consistent dates were validated and used in the age-depth model of core NEG18-06; 3 consistent dates were used for core NEG18-05, in addition to two dates from core NEG18-06 (*) thanks to core correlation based on XRF profiles (Figure SI-1).*

Core	Lab. code	Depth (cm)	^{14}C age (years BP)	Calibrated ^{14}C age 2σ range (cal BP)
NEG18-06	*Poz-108396*	*38*	*3375 ± 35*	*3548 – 3693*
NEG18-06	*Poz-108398*	*48.5*	*104.92 ± 0.33 pMC*	*(modern)*
NEG18-06	*Poz-108399*	*66.5*	*370 ± 30*	*424 – 498*
NEG18-06	*Poz-108400*	*94.5*	*5170 ± 40*	*5888 – 5999*
NEG18-06	*Poz-108401*	*105.4*	*3445 ± 30*	*3620 – 3734*
NEG18-06	*Poz-108402*	*140.5*	*1820 ± 30*	*1695 – 1797*
NEG18-06	Poz-118687	156.4	570 ± 30	588 – 642
NEG18-06*	Poz-118688	160.4	1070 ± 30	925 – 1006
NEG18-06	Poz-118565	164.4	1615 ± 30	1410 – 1539
NEG18-06	*Poz-108403*	*166.3*	*2385 ± 30*	*2345 – 2491*
NEG18-06*	Poz-118566	173.4	2595 ± 35	2701 – 2771
NEG18-06	Poz-108477	178.2	3480 ± 35	3686 – 3838
NEG18-06	Poz-118567	191.4	4550 ± 40	5050 – 5197
NEG18-06	Poz-108404	199	5660 ± 35	6388 – 6503
NEG18-06	Poz-118568	204.4	6130 ± 40	6931 – 7158
NEG18-06	Poz-108453	212.5	7890 ± 50	8590 – 8810
NEG18-05	Poz-126158	122	3645 ± 35	3874 – 4085
NEG18-05	Poz-126159	147	7160 ± 50	7920 – 8039
NEG18-05	Poz-126160	186	9680 ± 70	11,060 – 11,233

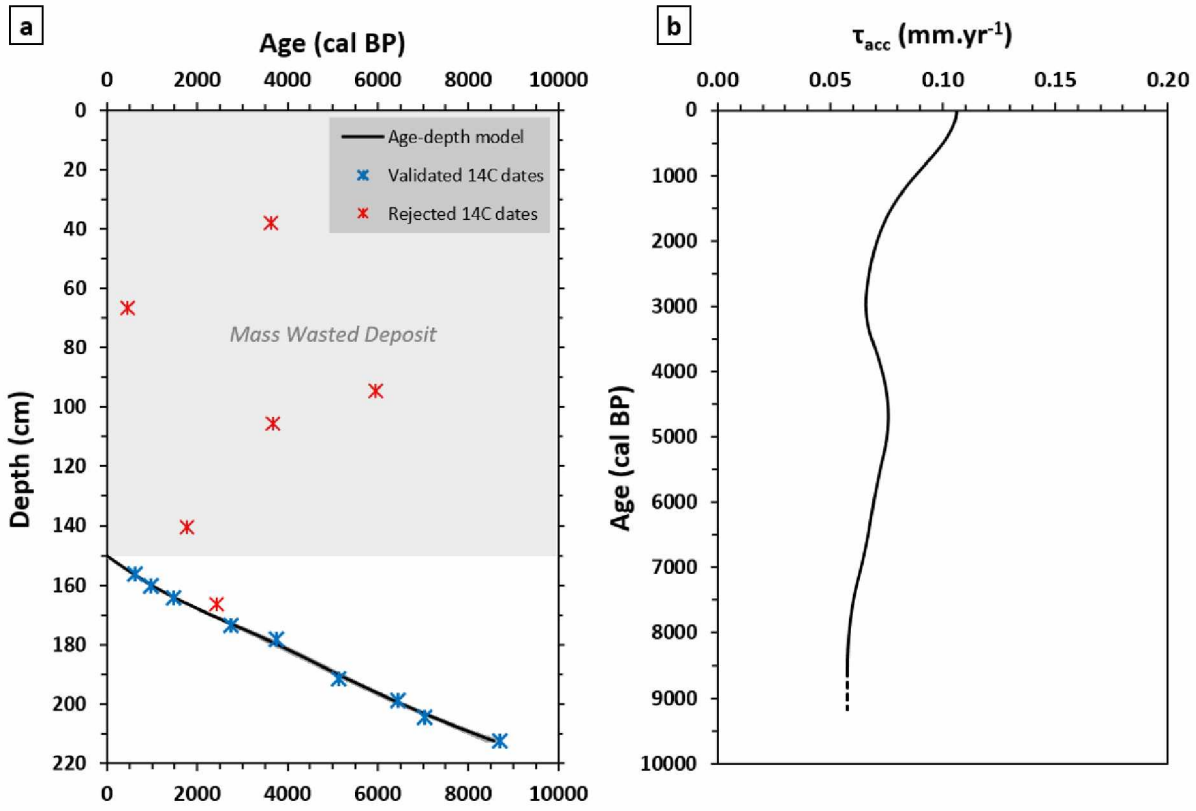

Figure 3 – Geochronology of core NEG18-06. *(a) Age-depth profile of core NEG18-06 as modeled by the* R *"clam" package (Blaauw, 2010) using calibrated* ^{14}C *ages, with uncertainties in grey shading; validated dates are shown in blue, rejected dates in red; Unit S (instantaneous mass wasted deposit) is represented in grey. (b) Sediment accumulation rate (*τ_{acc}*, in mm.yr*$^{-1}$*) of core NEG18-06 inferred from the age-depth model and extrapolated as constant over the last 600 years (dashed line).*

Because of the use of correlated ^{14}C dates from another core in its upper part, along with uncertainties on correlated depths caused by accidental drying, the age-depth model of core NEG18-05 (Figure SI-1) presents high age uncertainties estimated at ± 300 years. Thanks to a thinner Unit S (bottom at 90.3 cm depth), sediments of core NEG18-05 extend down to the beginning of the Holocene, the deepest radiocarbon age (186 cm) being measured at 11147 ± 87 cal BP. As for core NEG18-04 (Lefebvre et al., 2021), the top of Unit B on core 05 is marked by a hiatus of ~ 11.2 cm (corresponding to ~ 980 years) due to erosion by the mass wasted deposit, as attested by the absence of the modern Pb peak (Figure SI-1).

3.2 Weathering and erosion fluctuations over the Holocene

3.2.1 Physical erosion fluxes indicated by terrigenous inputs

High-resolution elemental XRF core-scanner profiles (14-year average steps) displayed in Figure 4 provide complementary information on the evolution of element fluxes over the last 9200 years in Lake Nègre. Titanium (Ti), which is well measured by XRF, is known to be a

lithogenic conservative element as well as Al, Zr and Rb for example (Boës et al., 2011) and is therefore a relevant proxy of terrigenous silicate inputs to lake sediments (Arnaud et al., 2012). Terrigenous fluxes inferred from Ti fluxes variations (Figure 4a) were stable between 9.2 and 5.7 kyr cal BP, during the Holocene Thermal Maximum, then slightly increased to a plateau until 4.2 kyr BP where a major rise in erosive fluxes is recorded. This shift is synchronous with the so-called "4.2 kyr BP event" recorded elsewhere in the Mediterranean area (Bini et al., 2019; Brisset et al., 2013) and characterized by global drying and cooling along with an intensification of extreme rainfall events (Sabatier et al., 2017; Wirth et al., 2013). After a short period of stability, erosive inputs increased again at 3.7 kyr BP before fluctuating until 1600 cal BP (AD 350), when a major erosive peak – with a twofold increase of Ti fluxes – is recorded until 1200 cal BP (AD 750) during the Early Middle Age ("Dark Ages"). The Mediaeval Climate Anomaly, corresponding to slightly increasing temperatures over Europe (Affolter et al., 2019), is characterized at first by lower terrigenous inputs between 1200 and 850 cal BP (AD 750-1100), followed by a bump of detrital fluxes at 850 cal BP (AD 1100) with a peak between 700 and 650 cal BP (AD 1250-1300). Detrital inputs then decrease at the onset of the Little Ice Age (LIA) before rising ultimately at 300 cal BP (AD 1650) to reach high modern levels. Most of the major increases in erosive fluxes coincide with glacier advances in the Southern Alps as recorded in the Ecrins-Pelvoux massif, especially at 4.2, 3.6, 1.3 and 0.87 kyr cal BP (Le Roy et al., 2017).

3.2.2 Characterization of the terrigenous inputs

Variations of the Ti content that reflects terrigenous inputs (Figure 3a) are well correlated to those of the Zr/Al ratio (Figure 4b, Figure SI-6) that is a raw indicator of grain size, as Zr is essentially incorporated in coarse zircon grains and Al in finer-grained minerals (clays) (Arnaud et al., 2016; Sabatier et al., 2017). In addition, negative correlations are observed between both Ti and Zr/Al and the K/Ti ratio (Figure 4c, Figures SI-7 and SI-8) that is known to decrease when increasing the degree of weathering of terrigenous inputs (Figure 3c, Figure SI-7) (Arnaud et al., 2012; Bajard et al., 2017a).

This indicates that the global rise of terrigenous inputs over the Late Holocene was accompanied by both a growing supply of coarse grains and of chemically weathered material from the watershed regolith. Such a rise has been evidenced in many other lakes in the Alps (Arnaud et al., 2016). This evolution corresponds to the onset of the Neoglacial and appears to be directly linked to climatic forcing such as rainfall and temperature, and more specifically to the increase in flood frequency as described in other Alpine lakes (Brisset et al., 2017; Sabatier et al., 2017; Wilhelm et al., 2012; Wirth et al., 2013). Globally, the trend of soil erosion in the Lake Nègre watershed can be described as follows, in agreement with other lakes in the French Alps (Brisset et al., 2013; Bajard et al., 2015): (i) very low detrital inputs in the Early to Mid-Holocene (9.2 to

4.2 kyr BP), probably due to soil stabilization by a developed vegetation and low extreme precipitation events; (ii) strong destabilization at the onset of the Neoglacial (4.2 kyr BP) due to increasing flood activity, resulting in inputs of moderately weathered material, originating from the incision of deeper soil horizons; (iii) globally increased erosion during the last 4200 years, supplying consistently more weathered material corresponding to soil sheet erosion. This regime shift is further strengthened by changes in the correlation relationships at 4.2 kyr BP (Figures SI-6, SI-7 and SI-8).

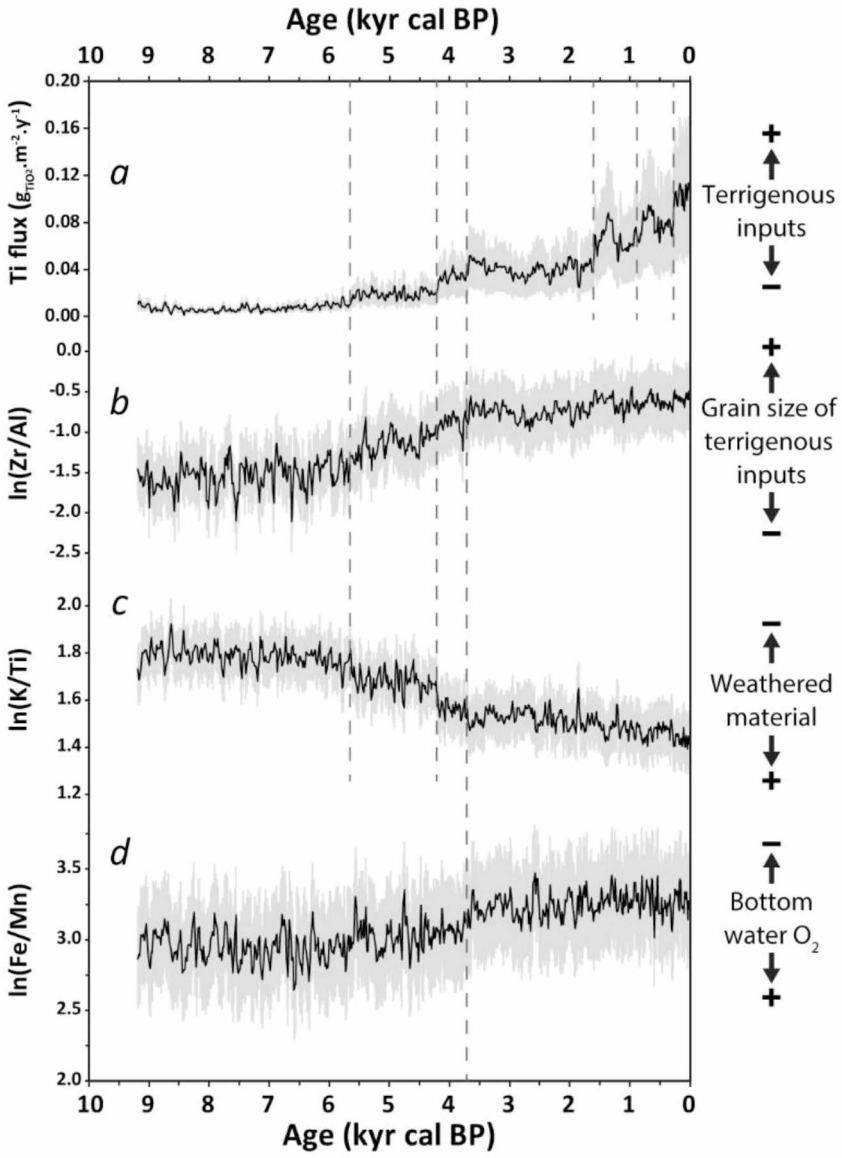

Figure 4 – XRF profiles of erosion and weathering indicators in Lake Nègre sediments over 9200 years. *(a) The flux (mass accumulation rate) of Titanium (Ti) is a proxy for terrigenous inputs; (b) ln(Zr/Al) (log ratio) is roughly correlated to the average grain size of terrigenous material; (c) ln(K/Ti) indicates the degree of weathering of terrigenous inputs; (d) ln(Fe/Mn) is an indicator of lake bottom water oxygenation at the time of deposition. Vertical grey dashed lines indicate major rises of terrigenous inputs and the concomitant evolution of other indicators. Grey shading corresponds to 2SD uncertainties.*

The global rise of terrigenous inputs over time resulted in a concomitant upcore increase of the sediment DBD (Figure 2), hiding the effects of sediment compaction that would have normally induced an inverse density profile. Anecdotally, peak inputs of coarser material could have resulted in slightly increasing sediment accumulation rates that could not be resolved in the smooth age-depth profile (Figure 3b): such potential effects would have further amplified elemental fluxes during peak terrigenous inputs.

In parallel to these climatic variations, oxygenation of the lake bottom water remained quite stable with a little decrease recorded at 3.7 kyr BP as witnessed by a slight increase of Fe/Mn in the sediments (Naeher et al., 2013) (Figure 4d). This trend is consistent with observations in Lake Robert in the French Alps (Elbaz-Poulichet et al., 2020).

The impact of human activities on erosion in the Lake Nègre catchment is hard to distinguish from climatic causes. Overall, the anthropogenic influence is thought to be low (if any), as the lake is remote from the current inhabited valleys and rather difficult to access. Moreover, the catchment relief and rocky cover prevents any crop culture. The human footprint should therefore have been restricted to limited pastoralism and deforestation. Although climatic factors should have been of primary importance in the variations of erosive fluxes described above, it is impossible to rule out anthropogenic impacts, that could have participated to or even triggered erosion increases, especially during the Bronze Age and the Middle Ages (Brisset et al., 2013; Giguet-Covex et al., 2014; Walsh et al., 2007).

3.3 Reconstructing past contributions of land-derived and autochthonous organic matter

In our first study on Lake Nègre sediments on two other cores spanning 3300 years (Lefebvre et al., 2021), we observed a strong correlation between total organic carbon and uranium accumulation. Additionally, ultrafiltration of the lake water showed that U was transported in the colloidal (< 0.2 µm) fraction. Based on these indicators, we inferred that U was transported into the lake via organic colloids that were subsequently deposited in the sediments. This hypothesis was strengthened by invariant $^{238}U/^{235}U$ isotopic ratios and by the association of non-crystalline U to organic moieties in the upper sediments. This finding shows that organic matter probably plays a major role in U mobility within the lake watershed, and in turn in U inputs to the sediments. In order to understand the variations in U accumulation through the Holocene, it therefore appeared necessary to characterize OM inputs and sources to the sediments.

3.3.1 Variations of bulk sedimentary OM inputs

The evolution of TOC deposition in Lake Nègre sediments over the last 9200 years is displayed in Figure 5. We observe substantial variations in the OM flux (F_{TOC}) over the Holocene, starting with an initial drop from 1.7 $g_{TOC}.m^{-2}.yr^{-1}$ to 1.2 $g_{TOC}.m^{-2}.yr^{-1}$ between 8.4 and 8.1 kyr BP, which could correspond to the 8.2 kyr BP cold event (Alley et al., 1997). After that, TOC inputs progressively increased twofold (up to 2.3 $g_{TOC}.m^{-2}.yr^{-1}$) from 8.2 to 3.5 kyr BP, with a period of peak OM accumulation between 7.2 and 6.3 kyr BP resulting in up to 19.4 wt% TOC. The deposition of organic compounds then decreased down to low levels (1.5 $g_{TOC}.m^{-2}.yr^{-1}$) stable from 2.2 to 1.0 kyr BP, before a slow increase over the last 1000 years up to 20th century levels of ~ 2 $g_{TOC}.m^{-2}.yr^{-1}$. Such variations over the Holocene may be caused by climate-driven fluctuations in OM production. For instance, the net decrease of OM inputs in the Late Holocene (after 3.5 kyr BP) could be related to lower temperatures during the Neoglacial that reduced vegetation development in the watershed or biomass productivity in the lake. In order to decipher the relative impact of OM sources variations, we estimated the contributions of global OM sources to total OM sedimentary inputs over the Holocene, as described in the next section.

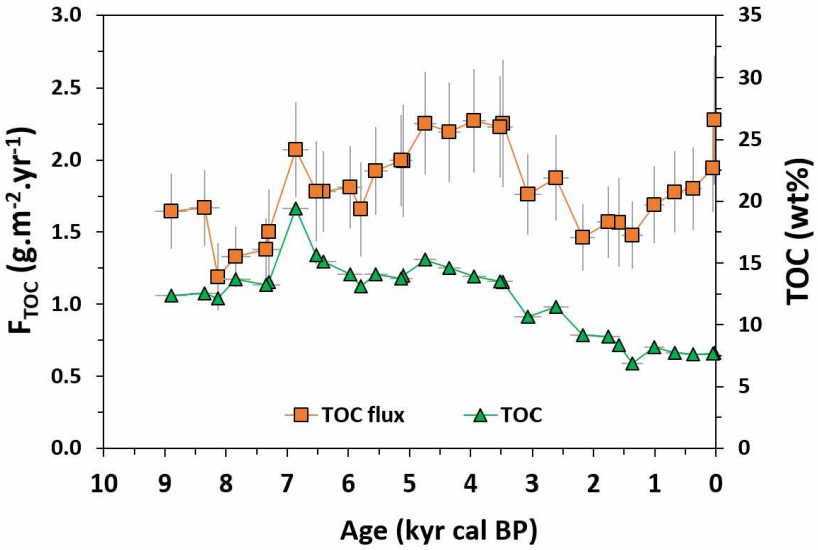

Figure 5 – Organic matter supply to Lake Nègre sediments over the Holocene. *Temporal evolution of Total organic carbon (TOC) content (wt%, in green) and TOC flux F_{TOC} ($g.m^{-2}.y^{-1}$, in orange). Error bars correspond to 2SD uncertainties.*

3.3.2 Contributions of autochthonous and terrigenous OM sources

Organic matter sources can be described at first order by two categories: autochthonous OM from primary production (algae and macrophytes) and terrigenous/land-derived OM from soils and land vegetation (Meyers and Teranes, 2001). Relative contributions from both sources can be assessed from biogeochemical proxies for which these sources have distinct signatures. Among such proxies are the widely-used C/N atomic ratio and $\delta^{13}C$ isotopic signature. Lacustrine

autochthonous OM resulting from primary production (phytoplankton and aquatic macrophytes) in the water column has a low C/N ratio typically between 6 and 9, while terrigenous OM originating from the watershed (in our case from the wetland zone at the lake inlet (Figure 1c), from meadows and poorly developed soils across the watershed) displays higher C/N ratios (Meyers and Teranes, 2001). From a paleo-environmental perspective and in the case of high-altitude alpine environments, terrigenous OM may originate from meadow-type environments with low-cellulose plants that are characterized by intermediate C/N ratios (typically between 13 and 15), and from heathland/forest environments with more cellulose-rich plants that will result in OM with higher C/N (ca. 17 and higher) (Meyers and Teranes, 2001; Seeber and Seeber, 2005). Even if at present only scattered trees are present in the watershed, during the early to mid-Holocene when temperatures were milder we cannot exclude the presence of more abundant trees at this altitude (Talon, 2010). The $\delta^{13}C$ signatures of lacustrine OM is less clearly defined in the literature and may be site-dependent. In their review, Meyers and Teranes indicate that, in contrast to marine OM, the $\delta^{13}C$ of lacustrine algae may not be clearly distinguishable from terrigenous OM, with comparable values between -25 and -30 ‰; under certain circumstances (supply of dissolved inorganic carbon with low $\delta^{13}C$), lacustrine algae may display lower isotopic signatures as low as -32 to -33 ‰ (Meyers and Teranes, 2001). On the other hand, modern algae from alpine Meidsee lake displayed less negative $\delta^{13}C$ signatures of ~ -15 ‰ (Thevenon et al., 2012). C4 plants have higher C/N and $\delta^{13}C$ compositions but they are not expected to be in significant proportion in the Alps (Pyankov et al., 2010). The isotopic signature of nitrogen ($\delta^{15}N$) may also be an indicator of OM sources but with more complicated interpretations (Meyers and Teranes, 2001).

All analyzed sediments (n = 22) display intermediary C/N ratios (between 9.8 and 15.8) and low $\delta^{13}C$ (-26.0 to -31.2 ‰) as shown in Figure 6a. The measured C/N ratios indicate at first order that the Lake Nègre sedimentary OM has always been composed of a mixture of autochthonous and land-derived organic material in comparable proportions over the Holocene. Nevertheless, the lack of clear co-variations between C/N, $\delta^{13}C$ and $\delta^{15}N$ (Figure 6a, Figure SI-9) prevents the use of isotopic signatures as an indicator of OM sources. In order to better decipher between terrigenous and autochthonous OM sources, we used Br as an additional proxy.

Because of the high affinity of bromine (Br) to organic matter (Leri et al., 2010; Leri and Myneni, 2012) and to diatoms in particular (Kerfoot et al., 1999; Phedorin et al., 2000), it has been shown that sedimentary Br amounts are closely related to OM accumulation, the Br/OM ratio being dependent on OM sources (Gilfedder et al., 2011; Guevara et al., 2019; Mayer et al., 2007, 1981; Ziegler et al., 2008). We therefore calculated semi-quantitative Br/TOC ratios by dividing Br obtained by XRF analysis (in fluorescence counts) by TOC contents (in wt%). No reliable

Br/TOC endmember values for OM sources in lacustrine environments could be found in the literature – in part because Br XRF signal depends on XRF counting time without Br calibration – but autochthonous organic matter is expected to accumulate more Br (i.e., display a higher Br/TOC) than terrigenous OM (Gilfedder et al., 2011; Mayer et al., 2007, 1981; Ziegler et al., 2008).

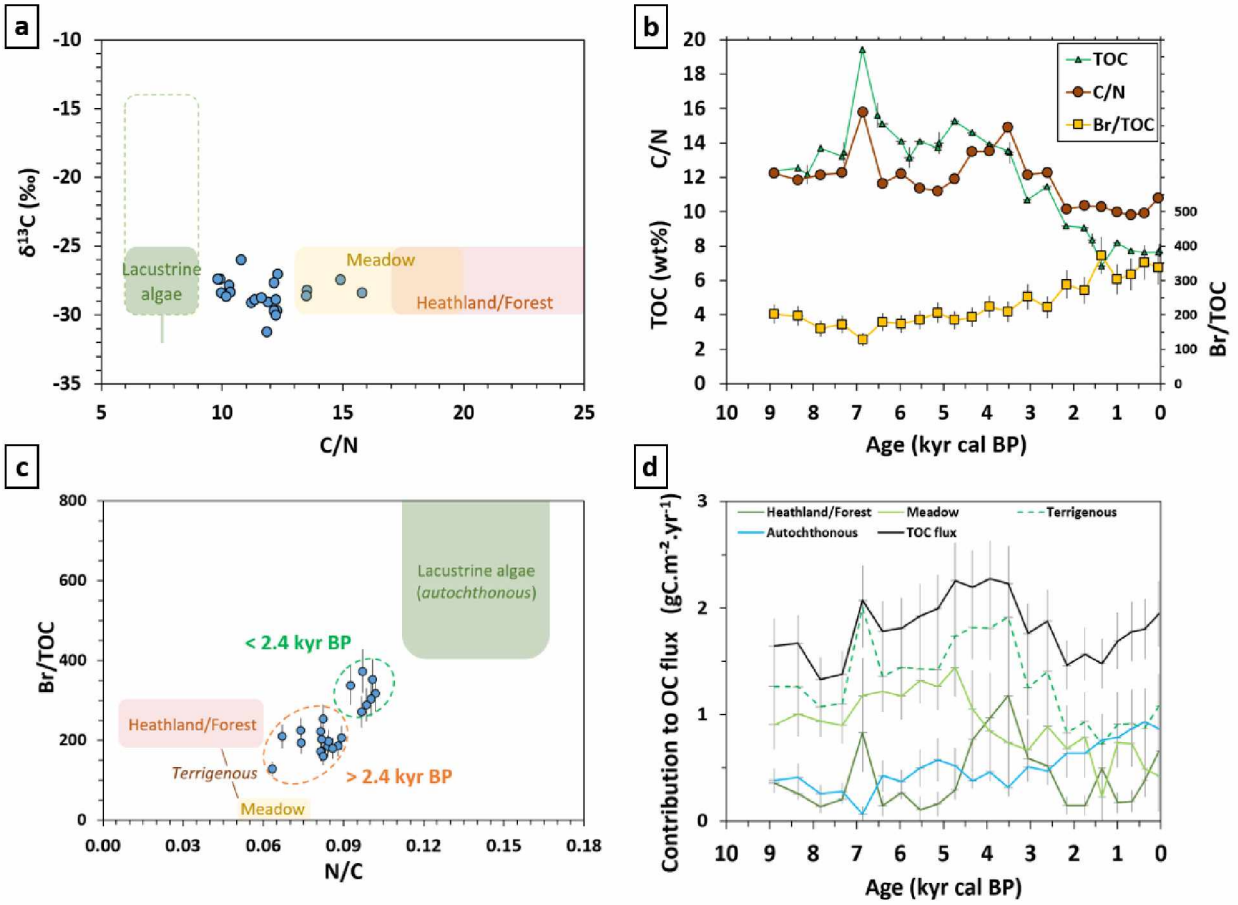

Figure 6 – Signatures and sources of organic matter (OM) in Lake Nègre sediments. *(a) $\delta^{13}C$ versus C/N signatures with OM sources endmembers from the literature (Meyers and Teranes, 2001; Seeber and Seeber, 2005; Thevenon et al., 2012); the $\delta^{13}C$ isotopic signature of lacustrine algae is expected between -25 and 30 ‰ or even down to -32 ‰ (Meyers and Teranes, 2001), but could also be less negative, up to -14 ‰ (Thevenon et al., 2012). (b) Evolution over time of C/N (red) and Br/TOC (yellow) signatures compared with TOC contents (green). (c) Br/TOC versus N/C signatures (to highlight potential mixing lines) with OM sources endmembers constrained by literature and experimental data; terrigenous OM comprises OM from both meadow- and heathland/forest-type environments; dashed ovals indicate sediments deposited before (orange) or after (green) 2.4 kyr cal BP. (d) Evolution over time of organic carbon (OC) fluxes to the sediments from the identified OM sources; terrigenous fluxes (dashed green) correspond to the sum of meadow- (light olive green) and heathland-originating (dark olive green) OM fluxes; total OC fluxes (black) correspond to the sum of autochthonous (blue) and terrigenous OM. Error bars indicate 2SD uncertainties.*

Consequently, the observed variations in the C/N and Br/TOC ratios over time in Lake Nègre sediments (Figure 6b) can be attributed to fluctuating contributions of OM sources. Br/TOC ratios appear to be roughly correlated to N/C ratios (Figure 6c), an observation that is consistent with literature data (e.g., Ziegler et al., 2008). Sediments deposited before ~ 2.4 kyr BP that

display low Br/TOC and relatively high C/N (i.e., low N/C) ratios can be clearly distinguished from those deposited after 2.4 kyr BP that show higher Br/TOC and lower C/N (i.e., higher N/C) ratios. These observations indicate that the relative contribution of terrigenous OM to total OM has decreased after 2.4 kyr BP. However, the data point scattering on Figure 6c suggests that a simple two-endmember mixing model – that would have resulted in a straight mixing line – cannot account for all samples. Three endmembers appear necessary to describe the whole dataset, as reported previously in marine sediments from the Gulf of Mexico (Gordon and Goñi, 2003). We thus ran a three-endmember mixing model, involving autochthonous OM and two terrigenous OM sources corresponding to past environments: meadow- and heathland/forest-type soils. Terrigenous contributions were consequently obtained by summing both contributions. The endmember values intervals displayed in Figure 6c were constrained both by literature data and by the sample values (see the discussion in SI). We took into account a range of endmember values (Table SI-1, Figure SI-10) that all show similar variations in the proportions of OM sources contributions (Figure SI-11). The results presented in Figure 6d correspond to the average contributions obtained with two representative sets of endmembers, namely "tight endmembers" with C/N and Br/TOC values as close as possible to the sediment data and "wide endmembers" with extreme values (Figure SI-12). The respective average endmember C/N and Br/TOC couples are 7 and 600 for autochthonous OM, 13.5 and 35 for meadow-derived OM and 60 and 225 for heathland/forest-derived OM. For comparison, a simple two-endmember mixing model (with a single terrigenous OM source) was also ran and showed comparable trends (Figures SI-13 to SI-16). It should be noted that the resulting contributions of the different OM types are associated to high uncertainties on their absolute values but are thought to be qualitatively consistent in terms of relative variations over the Holocene.

Our results indicate that the organic matter of Lake Nègre sediments has been dominated (between 70 and 100 %) by terrigenous inputs – especially from meadow environments – over most of the Holocene before 2.4 kyr BP, whereafter terrigenous and autochthonous OM reached similar proportions (~ 50 % each) (Figure 6d, Figure SI-12). Fluctuations in sedimentary OM contents were driven by variations in terrigenous OM inputs until 2.4 kyr BP, as lake primary production remained relatively low and stable over this period. A peak input of terrigenous OM occurred at 6.9 kyr BP, likely originating from the development of heathland or even forest soils, in agreement with the most important conifer forest extension in altitude in the Southern French Alps with an upper forest belt elevation between 2400 m and 2810 m (Talon, 2010). Another remarkable event is the period between ~ 4.5 and 2.4 kyr BP, when the watershed was covered by heathlands or forests. The quick drop of these land plant contributions after 3.5 kyr BP – that resulted in a global decrease of sedimentary OM accumulation – occurs simultaneously with a sharp increase of erosive inputs (Figure 4a) and could indicate a rapid forest opening as reported

elsewhere in the French Alps (Giguet-Covex et al., 2011; Bajard et al., 2017b), potentially due to either natural factors (e.g., treeline lowering due to decreasing temperature in the Neoglacial) or human-induced deforestation. This drop of terrigenous OM inputs starting at 3.5 kyr BP is concomitant with a progressive threefold increase of autochthonous primary production until reaching half of the sedimentary OM accumulation from 2.4 kyr BP to present. The growing diatom abundance resulting from increasing primary production is however not observable in the Si/Ti ratio variations (Figure SI-17), probably because of the major rise of erosive inputs that occurs simultaneously (Figure 4) and hides Si/Ti variations induced by diatom blooms (Chawchai et al., 2016; Martin-Puertas et al., 2012). One should keep in mind that although high relative variations in the quantity and composition of sedimentary inputs have been recorded over time, the sedimentation rate in such a high-altitude lake remained as low as ~0.1 $mm.yr^{-1}$ (Figure 3b).

The dominance of terrigenous OM inputs in the Mid-Holocene has been observed extensively in the Alps and corresponds to a period of enhanced soil development and soil stabilization by vegetation (Bajard et al., 2017b, 2015; Brisset et al., 2013; Elbaz-Poulichet et al., 2020; Mourier et al., 2010) that has been designated as the "Holocene Pedogenetic Optimum" in the French Northern Alps (Poulenard, 2011). The onset of the Neoglacial (Late Holocene) with a colder and wetter climate led to increasing erosion and a drop of sedimentary TOC coupled to a relative increase in the proportion of autochthonous OM (Elbaz-Poulichet et al., 2020; Giguet-Covex et al., 2011). Our observations are however contrasting with those recorded in sediments of more distant Lake Meidsee (Southwestern Swiss Alps) where organic matter was dominated by primary production prior to 5.1 kyr BP, the proportion of terrigenous OM increasing only after 5 kyr BP (Thevenon et al., 2012).

3.3.3 Responses of the lake watershed to climate changes over the Holocene

In the light of our results, in agreement with another study in this alpine area (Brisset et al., 2013), a history of the Lake Nègre catchment responses to climatic variations over the last 9200 years can be synthesized as follows:

1. From 9.2 to 4.2 kyr BP, corresponding to the Holocene Pedogenetic Optimum, the Lake Nègre watershed was characterized by low erosion and increasing terrigenous OM from alpine meadows, as a consequence of soil stabilization due to vegetation development and overall low precipitation. This stable period was occasionally marked by lower-scale variations, such as short-term fluctuations in OM accumulation (lowering during the 8.2 kyr BP event, increasing at 6.9 kyr BP) and a slight increase in terrigenous inputs at 5.7 kyr BP.

2. A major change in the lake environment occurred at the onset of the Neoglacial period, starting at 4.2 kyr BP with a major rise of erosive fluxes, and the sustained development of a heathland/forest-type vegetation. This change was further emphasized by another erosive event at 3.7 kyr BP associated to forest opening, probably responsible for the destabilization of the catchment soils. The latter event is also associated to a slight decrease of the lake bottom water oxygenation, that could be due to enhanced oxygen consumption by the coincidently growing primary production, caused by increasing nutrients supply by chemical erosion.
3. From ~3.5 kyr BP to present, the lake catchment showed a higher sensitivity to climatic changes, as soil erosion remained at higher levels than prior to 4.2 kyr BP and even further increased over the last 1600 years, with a high sensitivity to centennial climatic variations (Dark Ages, Middle Ages, LIA). Primary production continuously increased, as a probable consequence of persisting higher nutrient supply by erosive inputs. The impact of human activities on this erosion increase cannot be deciphered and may have played a significant role like elsewhere in the Mediterranean Alps, especially in the past 1600 years (Brisset et al., 2017, 2015, 2013).

3.4 Fluctuations of OM-bound uranium inputs to Lake Nègre over the Holocene

3.4.1 Assessment of U sources, transport and deposition in the sediments

Over the past 9200 years, sedimentary U concentrations of core NEG18-06 were exceptionally high and continuously decreased by a factor of three, from ~ 1100-1200 to ~ 350 $\mu g.g^{-1}$ (Figure 7a). Such U contents in natural lake sediments are unexpected compared to typical sedimentary ranges and to the watershed background rocks (Lefebvre et al., 2021). Thanks to these high U amounts, we could measure the uranium profile at high temporal resolution (time steps 10-20 years) using the quick and cost-effective XRF core-scanner technique. A 20-year resolution U profile was measured in Lake Baikal sediments by (Phedorin and Goldberg, 2005) but with less accessible and more time-consuming synchrotron-radiation XRF (SR-XRF). In the latter study, low U concentrations (< 30 µg/g) resulted in a higher discrepancy between XRF and ICP-MS measurements.

The XRF profile of U, calibrated with ICP-MS data, for the well-preserved and long core NEG18-06 is consistent with similar measurements performed on the NEG18-07 core (Lefebvre et al., 2021) and by gamma spectrometry data on core NEG18-05 (this study), as shown in Figure 7a. The high resolution profile from core NEG18-07 spanning 3300 years closely matches that of core NEG18-06, with a little offset attributed to differences in sedimentation rates and/or

sediment density. In particular, centennial-scale U fluctuations due to climatic variations over the last 2000 years as described above are also recorded on this core. Furthermore, the first order variations of U profiles in cores NEG18-05 and NEG18-06 are in good agreement. Core NEG18-05 additionally offers the opportunity to go further back in time, up to 11.2 kyr BP. Gamma spectrometry measurements show a net increase of U accumulation between 11.2 and 9.1 kyr BP, at the onset of the Holocene, up to ~ 1250 µg/g at 9.1 kyr BP.

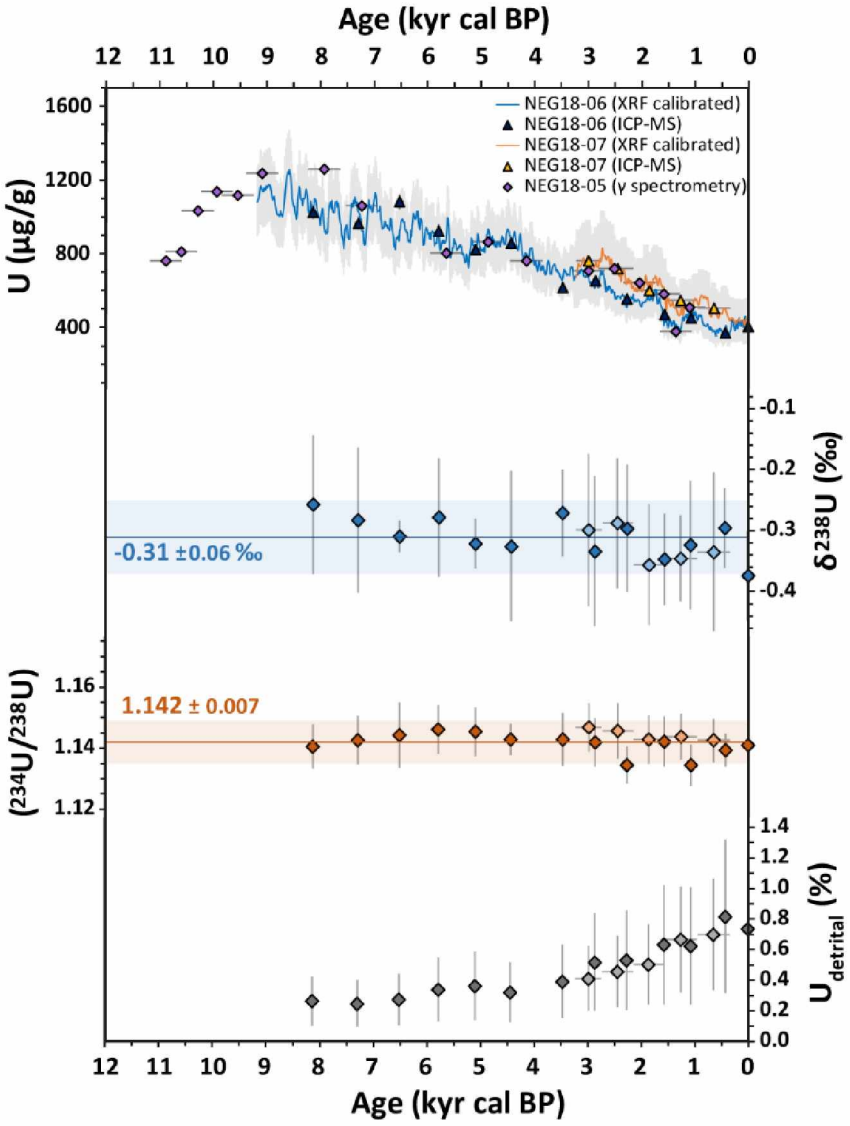

Figure 7 – Evolution of uranium geochemical proxies in Lake Nègre sediments over 9200 years. *(a) Uranium concentrations (µg/g) measured in three sediments cores taken in the same area of Lake Nègre: NEG18-06 (blue), NEG18-07 (orange) and NEG18-05 (purple); U signals from XRF were calibrated with concentration data from ICP-MS for cores NEG18-06 and -07 (triangles); on core NEG18-05, U was measured by gamma spectrometry (purple diamonds). (b) $\delta^{238}U$ isotopic signatures, with an average value of -0.31 ± 0.06 ‰ (blue line, 2SD uncertainties in blue shading). (c) ($^{234}U/^{238}U$) activity ratios, with an average value of 1.142 ± 0.007 (orange line, 2SD uncertainties in orange shading). (d) Detrital U fraction ($U_{detrital}$, in % of total U) inferred from U/Th ratios. In (b) to (d) figures, dark diamonds correspond to samples from core NEG18-06 (this study), light diamonds from NEG18-07 (Lefebvre et al., 2021). Error bars indicate 2SD uncertainties.*

The sources and modes of deposition of U in Lake Nègre sediments were investigated using U isotopic signatures (Figure 7). The trend observed over 3300 years on core NEG18-07 (Lefebvre et al., 2021) is consistent over the entire 9200-year period on core NEG18-06. Mixing equations based on $^{238}U/^{232}Th$ ratios showed that the exceptional amounts of sedimentary U are non-detrital (> 99 %, Figure 7d). We observe a slight increase in detrital U fractions over time that is attributed to the concomitant global increase in detrital inputs as inferred from Ti fluxes (Figure 4a). Constant ($^{234}U/^{238}U$) activity ratios along the core, with an average value equal to 1.142 ± 0.007 (Figure 7c), indicate that U consistently originated from chemical weathering of the watershed granitic rocks and was initially transported under dissolved forms (Andersen et al., 2009; Chabaux et al., 2003). $^{238}U/^{235}U$ ratios (expressed as $\delta^{238}U$) also display constant values (average -0.31 ± 0.06 ‰) along the core within uncertainties (Figure 7b). This signature, which is a proxy of U redox and sorption reactions (see the review by Andersen et al., 2017), is in the range of the watershed granite and slightly lower than the lake inlet water (Lefebvre et al., 2021). This result underlines the potential role of U adsorption onto suspended particles in the lake water column (Hinojosa et al., 2016) and excludes any substantial contribution from dissolved U(VI) reduction when penetrating the sediment pore water (e.g., Andersen et al., 2014). In conclusion, despite variations in amplitude, the nature of U inputs (from transport to deposition) to Lake Nègre sediments remained comparable over the last 9200 years.

Although climatic variations occurred through the Holocene, we do not observe variations in the ($^{234}U/^{238}U$) signature like those noted by Goldberg et al. (2010) in Lake Baikal sediments over the past 150 kyr. In the latter study, significant variations in authigenic ($^{234}U/^{238}U$) concomitant with major climatic changes such as Glacial and Interglacial periods were explained by climate-induced redistribution of rivers discharge over the large Lake Baikal watershed, resulting in variable U sources to the lake. The small size of the Lake Nègre catchment and the relative homogeneity of its bedrock (Lefebvre et al., 2021), combined with less intense climatic variations during the Holocene with respect to those of the last 150 kyr, explain the absence of resolvable isotopic variability in non-detrital U inputs.

3.4.2 Variations in U fluxes to the sediments

The evolution of U inputs to Lake Nègre sediments over most of the Holocene can be interpreted in the light of the variations in the sediment biogeochemical characteristics described above. A high-resolution profile of U mass accumulation rate – i.e., U flux (F_U) – over the Holocene, as calculated from calibrated XRF core-scanner data, is shown in Figure 8a. Uranium fluxes varied less than U concentrations because sediment density and accumulation rates globally increased over time, balancing the decreasing U contents. A major decrease in U accumulation is observed from 9.2 to ~7 kyr BP, followed by an increase until ~4.5 kyr BP, a second drop from 4.5 to 2.5 kyr

BP and a last increase until present, especially in the last 500 years. Overall, the Holocene trend of U flux roughly resembles that of temperature in the Alpine region (Figure 8b, Figure SI-18; adapted from Heiri *et al.* (2015)). The most remarkable common feature is the main bump around 4.5 kyr BP in both U flux and temperature. Shorter-scale U fluctuations are also recorded, especially in the past two millennia, that coincide with climatic variations not well recorded in the chironomid record of Heiri *et al.* (2015) (Figure 8b) but widely reported in Europe (e.g., Affolter et al., 2019): higher U supply occurred during warm periods (Roman, Mediaeval and modern periods) and lower U flux during colder phases (Dark Ages, LIA) (Figure 8a). Although U fluxes could not be calculated on low-resolution core NEG18-05, an increase in U concentrations was noted in the Early Holocene (Figure 7a). During this period, temperatures continued to rise after the quick warming at the end of the Younger Dryas, up to maximal temperatures corresponding to the Holocene Thermal Maximum (Affolter et al., 2019; Heiri et al., 2015; Samartin et al., 2017). This finding is again in agreement with the correspondence between increasing temperature and higher U accumulation.

Overall, the average U flux to Lake Nègre sediments over the Holocene was equal to 10.7 ± 3.0 $mg_U.m^{-2}.yr^{-1}$, equivalent to 4.5 ± 1.3 $nmol_U.cm^{-2}.yr^{-1}$. Although on a different spatial scale, this flux is for instance ~ 20 times greater than U fluxes to the California margin (McManus et al., 2005) and more than two orders of magnitude higher than U fluxes to the Black Sea sediments (Anderson et al., 1989).

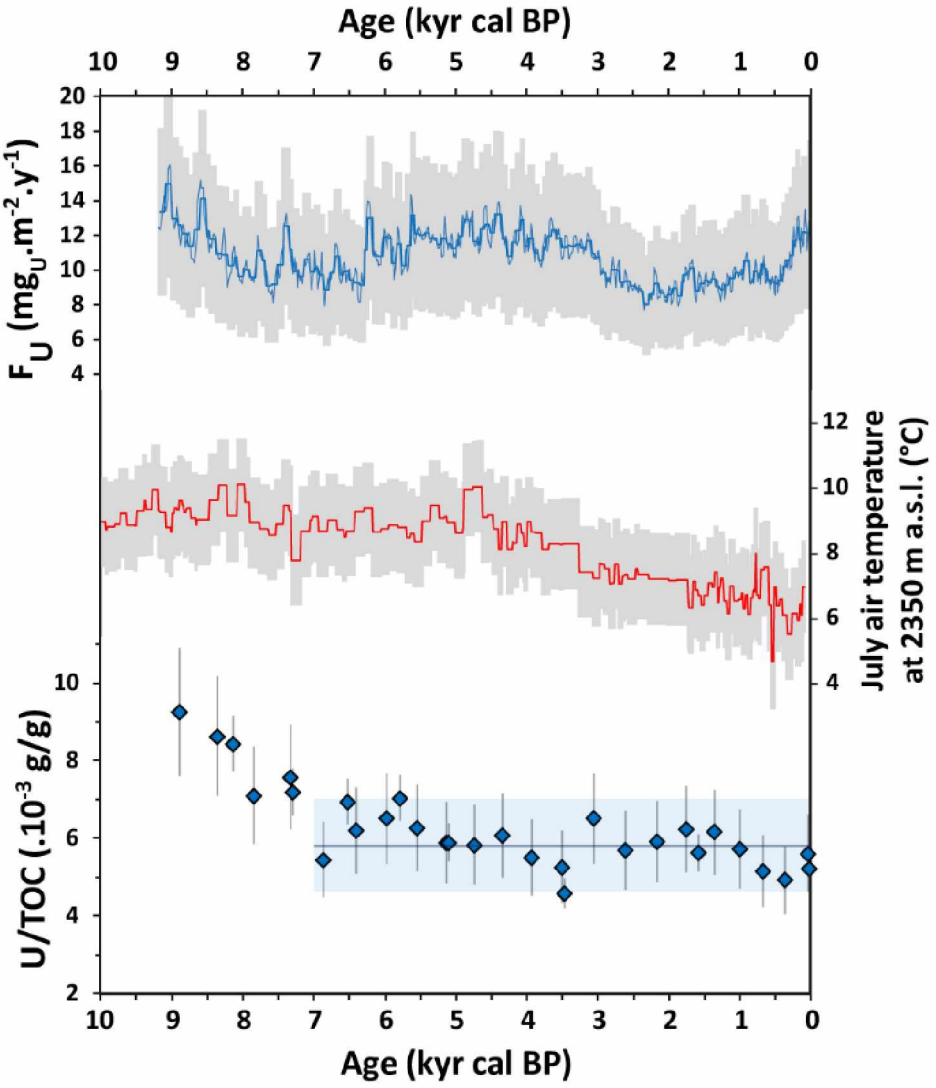

Figure 8 – U flux (F_U) to Lake Nègre sediments, compared to temperature and OM supply. *(a) Evolution over time of U fluxes over 9200 years, at high resolution from XRF measurements (thin blue line) and with 5-point averages (thick blue line). (b) Evolution of July air temperatures at 2350 m above sea level (a.s.l.) for the Alpine region over the past 10,000 years inferred from chironomid records, adapted from Heiri et al. (2015) with a temperature lapse rate of 6 °C per 1000 m. (c) Evolution of U/TOC ratios over the past 9200 years, with an average value of 5.8 ± 1.2 $mg_U.g_{TOC}^{-1}$ for the last 7 kyr BP (blue line). Error bars and shading correspond to 2SD uncertainties.*

3.4.3 Organic matter controls on U supply and deposition in the sediments

Lefebvre *et al.* (2021) demonstrated from sequential ultra-filtration analysis along with geochemical and isotopic proxies that U was probably associated to organic colloids in the Lake Nègre water before settling down in the sediments. This finding was consistent with the solid-state U speciation of recently deposited sediments in this lake, consisting of non-crystalline U bound to organic moieties (Lefebvre et al., 2021). In this light, the association of U to OM was investigated through the evolution of U/TOC ratios. Sedimentary U/TOC decreased in the Early

Holocene until ~7 kyr BP and then remained rather stable until present, with an average value of 5.8 ± 1.2 $mg_U.g_{TOC}^{-1}$ (Figure 8c, Figure SI-19). Such a correlation between non-detrital U and TOC accumulation was observed in the sediments of Lake Holland in Eastern Canada (Chappaz et al., 2010) and in oceanic environments (Anderson et al., 1998; Chase et al., 2001; McManus et al., 2005; Zheng et al., 2002). Considering the substantial fluctuations of U and TOC contents alone (Figure 5 and 8a), this observation tends to show that after a transitory period in the aftermath of the Late Glacial period, U association to organic matter followed a similar pattern over the last 7000 years.

In more detail, it appears that U accumulation is well correlated to the contribution of meadows to bulk OM ($R^2 = 0.88$, $p < 10^{-5}$), and more globally to terrigenous OM ($R^2 = 0.89$, $p < 10^{-5}$) after 7 kyr BP (Figure 9). For heathland/forest environments, periods of negligible contributions (≤ 2 wt%) show no relationship with U, while periods of forest development (especially at 6.9 kyr BP and between 4.5 and 2.4 kyr BP) are associated to a similar U enrichment than meadow-type environments. In contrast, there is no apparent link between lake primary productivity and U accumulation. Overall, these trends tend to demonstrate that U supply to Lake Nègre sediments has been controlled by the supply of terrigenous OM for the last 7000 years. Moreover, one may infer that U was initially trapped in soils because of its affinity to the soil organic compounds (e.g., Owen and Otton, 1995), before being exported to the lake by soil erosion, under the form of U bound to organic colloids and particles (Regenspurg et al., 2010; Wang et al., 2013). This hypothesis is consistent with the ability of mountainous soils and wetlands to naturally accumulate high quantities of U (Owen and Otton, 1995; Peña et al., 2020; Regenspurg et al., 2010). However, it is seemingly contrasting with data from Lake Baikal where U seems to preferentially bind – if at all – to autochthonous OM (Och et al., 2016).

In this light, fluctuations of the U flux (Figure 8a) after 7 kyr BP can be directly linked to variations in the development of soils and vegetation and thus in terrigenous OM supply to the lake (Figure 6d). The period of high U flux values culminating at ~4.5 kyr BP corresponds to the Holocene Pedogenetic Optimum (Poulenard, 2011) where soils were more developed and accumulated more U, resulting in higher U supply to the lake through soil erosion. At the onset of the Neoglacial, the lower development and accentuated weathering of soils (Figure 4) caused a global lowering of U fluxes, with slight increases during warmer periods.

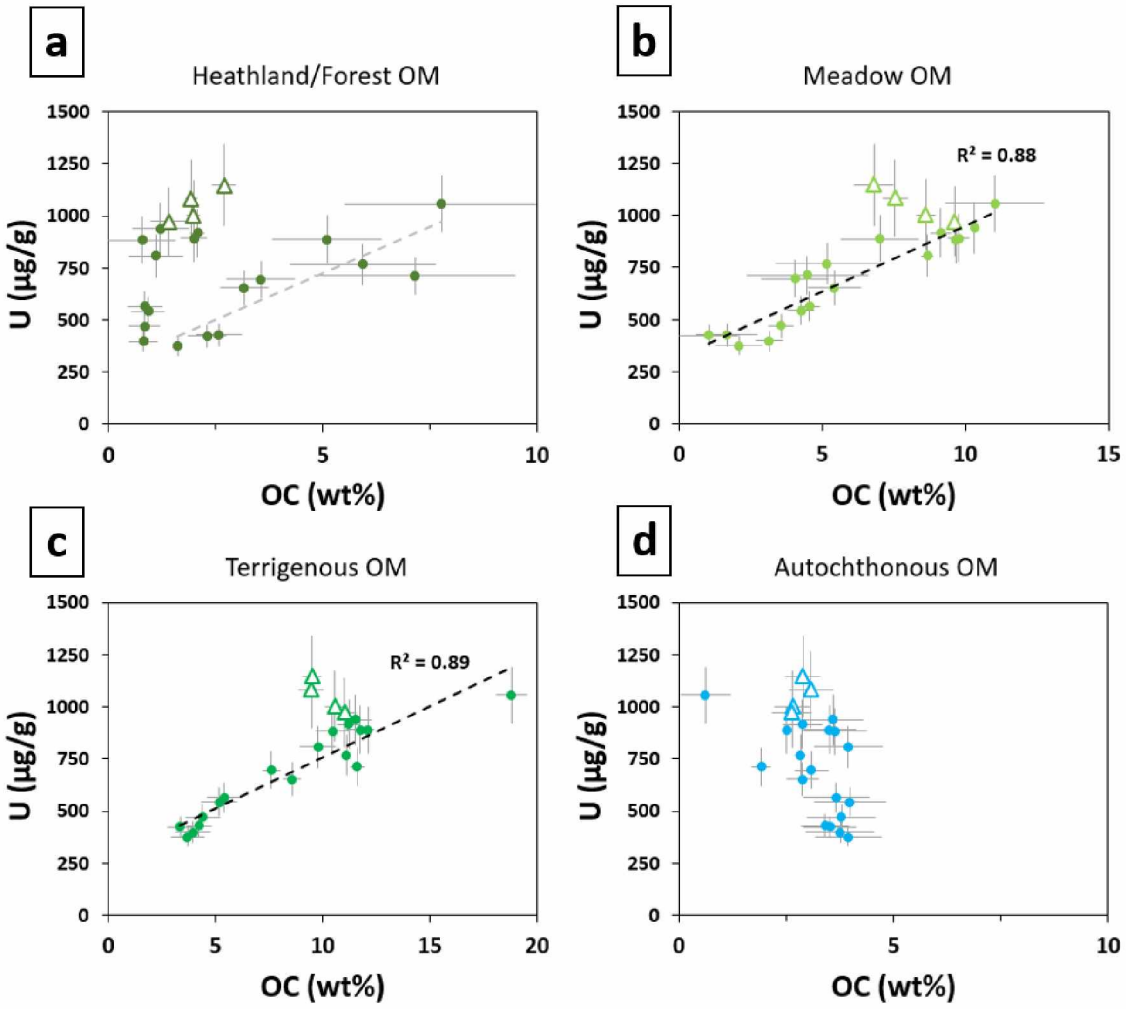

Figure 9 – Impact of OM sources on U supply to the sediments. *Relationship between bulk sedimentary U and OC contribution from each OM source, as calculated from C/N and Br/TOC ratios (section 3.3.2, Figure 5d), before (open triangles) and after (solid circles) 7 kyr BP: (a) Heathland/forest environments, (b) Meadows, (c) Terrigenous OM (sum of heathlands and meadows) and (d) autochthonous OM. For meadow environments and terrigenous OM after 7 kyr BP, a linear relationship is observed (black dashed lined), with corresponding correlation coefficients R^2. For heathland environments, a potential trend (when the OC contribution is significant) is indicated by a grey dashed line. Error bars correspond to 2SD uncertainties.*

After U entered the lake water, carried by terrigenous organic particles, additional processes may occur such as desorption followed by adsorption on other particles such as algae (Fisher et al., 1987; Kalin et al., 2005; Mann and Fyfe, 1985, 1984). The potential involvement of inorganic particles in U sedimentation is considered minor as no positive correlation was observed between U and Fe, Zr, Si or Al (Figure SI-20). However, understanding the processes controlling U deposition in the sediments from the lake water would require further investigation of the water column with isotopic proxies ($\delta^{238}U$). It is noteworthy to indicate that U scavenging in the lake sediments is not quantitative, as a significant dissolved U proportion is exported through the lake outlet that contains U concentrations only slightly inferior to those of the lake inlet water (2.3 ± 0.1 and 2.6 ± 0.1 $\mu g.L^{-1}$ respectively (Lefebvre et al., 2021)).

In summary, organic matter probably plays a dual role in the control of sedimentary U accumulation, through (i) the control of U supply to the lake (bound to terrigenous OM) and (ii) the hypothetical control of U fixation and settlement in the water column (by all types of OM) through exchanges between the dissolved and suspended U pools. A minor contribution from dissolved U(VI) reduction at the sediment-water interface cannot be excluded.

3.4.4 A transitory period in U association to OM before 7 kyr BP

A period of particular interest is the transitory interval between 9.2 and 7 kyr BP when U/TOC decreased before reaching its constant level of 5.8 ± 1.2 $mg_{U}.g_{TOC}^{-1}$ (Figure 8c). No significant change in erosion and weathering processes is detected during this period (Figure 4). This drop appears to be caused by a decrease of the U supply (-30 % of the U flux, Figure 8a) that is relatively higher than the terrigenous organic carbon (OC) decrease (-15 % of the terrigenous OC flux, Figure 6d) and may thus find its origin in the evolution of a specific U-controlling process. Considering that the main evolution in the distribution of OM sources is a moderately growing contribution of meadow-type OM inputs (Figure 6d), a possible explanation is that this transition reflected the development of the wetland upstream of the lake (Figure 1c). This wetland may act as a hotspot of U scavenging among the soils of the watershed (Regenspurg et al., 2010) and retain a significant fraction of U fluxes (Owen and Otton, 1995) before exporting lower U amounts associated to OM, by erosion. A less developed wetland in the Early Holocene after the Late Glacial period would have been less efficient in terms of U filtration on its path to the lake, resulting in exceeding U inputs to the lake. In such a case, this excess fraction of U inputs would not be associated to terrigenous OM and would enter the lake as dissolved (potentially complexed) U species. An additional mechanism of U scavenging in the sediments may then have been at stake, ultimately resulting in a higher U/OM ratio, such as adsorption to OM with higher U affinity (such as autochthonous OM), or another unidentified mechanism such as dissolved U(VI) reduction and precipitation at the sediment-water interface that could not be detected with our low temporal resolution $\delta^{238}U$ analysis (only two data points older than 7 kyr BP). In this scenario, the wetland would have been fully established about 7000 years ago, with a stable U scavenging process, leading to constant U/TOC ratios in the sediments until present.

Another hypothesis is that the deglaciation 13,000-14,500 years ago (Brisset et al., 2015, 2014) could have exposed an important source of U-enriched material, resulting in excess U supply compared to terrigenous OM production. Under such circumstances, the transitory period would have lasted several thousand years, until U supply from the watershed reached a stable level.

4. Environmental implications

Through the description of the fluctuations in mineral and organic inputs to the sediments of Lake Nègre, our study underlines the major impacts of Holocene climatic variations on weathering and erosion regimes as well as vegetation development in a small, high-altitude watershed. Regime shifts in rainfall and temperature such as those recorded at 4.2 and 3.7 kyr BP have substantial impacts on the supply of detrital material and on the relative development of terrestrial vegetation and lacustrine biomass.

One of the main findings of this study is that U accumulation in Lake Nègre sediments is not controlled by water oxygenation. High fluctuations in U supply are recorded while the lake bottom water oxygenation remained almost constant as attested by the Fe/Mn ratio (Figure 4d). This observation questions the use of U concentrations (and potentially of other redox-sensitive metals with high affinity to OM, such as molybdenum) as a reliable proxy for bottom water O_2. Other tracers such as U and Mo isotopes ($\delta^{238}U$ and $\delta^{98}Mo$) (Asael et al., 2013; Brüske et al., 2020) or Fe/Mn ratio (e.g., Naeher et al., 2013) should be measured in parallel to ensure that U (or Mo) variations are not driven by OM fluxes rather than bottom O_2. For example, intervals of high U, Mo and S accumulation in sediments of Crevice Lake (USA) are interpreted as markers of past year-round anoxia (Whitlock et al., 2012). However, these elements are well correlated to TOC contents, and might thus be indicators of high OM supply rather than water oxygen deficiency.

Our multi-proxy study also strengthens the identification of factors controlling U enrichments and may contribute to the understanding of the formation of sedimentary U ores, which often display an association between U and OM (Cumberland et al., 2016; Landais, 1996; Spirakis, 1996).

Several questions about the U cycle in the Lake Nègre watershed remain unanswered. For example, the original source of uranium is still unidentified. ($^{234}U/^{238}U$) activity ratios show that U initially originates from weathering of the watershed granites. However, as sampled granites contain relatively low U amounts (Lefebvre et al., 2021), it is impossible to determine if such a high U supply to the lake is caused either by weathering of large volumes of background rocks, for example through an extended network of fractures, or by U dissolution from an unidentified U-enriched rock body. Additionally, intermediate U accumulation zones between the bedrock and the lake – acting as secondary U sources to the lake – may be at stake, especially the wetland located right upstream of the lake which potential role in U sequestration has been discussed above. Finally, a persisting grey area is the behavior of U within the water column, between its supply through the lake inlet and wetland to its deposition in the bottom lake sediments.

Acknowledgements

We thank Gilles Alcalde, Cyrielle Jardin, Mathilde Zebracki and Pascale Blanchart (IRSN), Emmanuel Malet (EDYTEM), Didier Jézéquel and Barthélémy Julien (IPGP) for their help in sampling and chemical analyses. We thank Thierry Allard (IMPMC) for assistance in U-bearing samples handling at IMPMC. The Parc National du Mercantour is greatly acknowledged for having provided access and sampling authorizations to Lake Nègre. Funding: this work was supported by IRSN through collaborative research program n° LS 20942; by the Programme National EC2CO-BIOHEFECT/ECODYN (PUMA); by IPGP multidisciplinary program PARI; and by Paris–IdF Region [SESAME Grant no. 12015908]. This study contributes to the IdEx Université de Paris ANR-18-IDEX-0001. This is PATERSON, the IRSN's mass spectrometry platform, contribution no. 10.

This paper is dedicated to all victims of the floods of October 2020 in the Vésubie Valley.

REFERENCES

Affolter, S., Häuselmann, A., Fleitmann, D., Edwards, R.L., Cheng, H., Leuenberger, M., 2019. Central Europe temperature constrained by speleothem fluid inclusion water isotopes over the past 14,000 years. Sci. Adv. 5, eaav3809. https://doi.org/10.1126/sciadv.aav3809

Alley, R.B., Mayewski, P.A., Sowers, T., Stuiver, M., Taylor, K.C., Clark, P.U., 1997. Holocene climatic instability: A prominent, widespread event 8200 yr ago. Geology 25, 483–486. https://doi.org/10.1130/0091-7613(1997)025<0483:HCIAPW>2.3.CO;2

Andersen, M.B., Erel, Y., Bourdon, B., 2009. Experimental evidence for 234U–238U fractionation during granite weathering with implications for 234U/238U in natural waters. Geochim. Cosmochim. Acta 73, 4124–4141. https://doi.org/10.1016/j.gca.2009.04.020

Andersen, M.B., Romaniello, S., Vance, D., Little, S.H., Herdman, R., Lyons, T.W., 2014. A modern framework for the interpretation of 238U/235U in studies of ancient ocean redox. Earth Planet. Sci. Lett. 400, 184–194. https://doi.org/10.1016/j.epsl.2014.05.051

Andersen, M.B., Stirling, C.H., Weyer, S., 2017. Uranium Isotope Fractionation. Rev. Mineral. Geochem. 82, 799–850. https://doi.org/10.2138/rmg.2017.82.19

Anderson, R.F., Fleisher, M.Q., LeHuray, A.P., 1989. Concentration, oxidation state, and particulate flux of uranium in the Black Sea. Geochim. Cosmochim. Acta 53, 2215–2224. https://doi.org/10.1016/0016-7037(89)90345-1

Anderson, R.F., Kumar, N., Mortlock, R.A., Froelich, P.N., Kubik, P., Dittrich-Hannen, B., Suter, M., 1998. Late-Quaternary changes in productivity of the Southern Ocean. J. Mar. Syst. 17, 497–514. https://doi.org/10.1016/S0924-7963(98)00060-8

Arnaud, F., Poulenard, J., Giguet-Covex, C., Wilhelm, B., Révillon, S., Jenny, J.-P., Revel, M., Enters, D., Bajard, M., Fouinat, L., Doyen, E., Simonneau, A., Pignol, C., Chapron, E., Vannière, B., Sabatier, P., 2016. Erosion under climate and human pressures: An alpine lake sediment perspective. Quat. Sci. Rev. 152, 1–18. https://doi.org/10.1016/j.quascirev.2016.09.018

Arnaud, F., Révillon, S., Debret, M., Revel, M., Chapron, E., Jacob, J., Giguet-Covex, C., Poulenard, J., Magny, M., 2012. Lake Bourget regional erosion patterns reconstruction reveals Holocene NW European Alps soil evolution and paleohydrology. Quat. Sci. Rev. 51, 81–92. https://doi.org/10.1016/j.quascirev.2012.07.025

Asael, D., Tissot, F.L.H., Reinhard, C.T., Rouxel, O., Dauphas, N., Lyons, T.W., Ponzevera, E., Liorzou, C., Chéron, S., 2013. Coupled molybdenum, iron and uranium stable isotopes as oceanic paleoredox proxies during the Paleoproterozoic Shunga Event. Chem. Geol., Special Issue dedicated to H.D. Holland: Evolution of the atmosphere and ocean through time 362, 193–210. https://doi.org/10.1016/j.chemgeo.2013.08.003

Bajard, M., Poulenard, J., Sabatier, P., Develle, A.-L., Giguet-Covex, C., Jacob, J., Crouzet, C., David, F., Pignol, C., Arnaud, F., 2017a. Progressive and regressive soil evolution phases in the Anthropocene. CATENA 150, 39–52. https://doi.org/10.1016/j.catena.2016.11.001

Bajard, M., Poulenard, J., Sabatier, P., Etienne, D., Ficetola, F., Chen, W., Gielly, L., Taberlet, P., Develle, A.-L., Rey, P.-J., Moulin, B., de Beaulieu, J.-L., Arnaud, F., 2017b. Long-term changes in alpine pedogenetic processes: Effect of millennial agro-pastoralism activities (French-Italian Alps). Geoderma 306, 217–236. https://doi.org/10.1016/j.geoderma.2017.07.005

Bajard, M., Sabatier, P., David, F., Develle, A.-L., Reyss, J.-L., Fanget, B., Malet, E., Arnaud, D., Augustin, L., Crouzet, C., Poulenard, J., Arnaud, F., 2015. Erosion record in Lake La Thuile sediments (Prealps, France): Evidence of montane landscape dynamics throughout the Holocene: The Holocene. https://doi.org/10.1177/0959683615609750

Barnes, C.E., Cochran, J.K., 1990. Uranium removal in oceanic sediments and the oceanic U balance. Earth Planet. Sci. Lett. 97, 94–101. https://doi.org/10.1016/0012-821X(90)90101-3

Beniston, M., 2006. Mountain Weather and Climate: A General Overview and a Focus on Climatic Change in the Alps. Hydrobiologia 562, 3–16. https://doi.org/10.1007/s10750-005-1802-0

Bini, M., Zanchetta, G., Perşoiu, A., Cartier, R., Català, A., Cacho, I., Dean, J.R., Rita, F.D., Drysdale, R.N., Finnè, M., Isola, I., Jalali, B., Lirer, F., Magri, D., Masi, A., Marks, L., Mercuri, A.M., Peyron, O., Sadori, L., Sicre, M.-A., Welc, F., Zielhofer, C., Brisset, E., 2019. The 4.2 ka BP Event in the Mediterranean region: an overview. Clim. Past 15, 555–577. https://doi.org/10.5194/cp-15-555-2019

Blaauw, M., 2010. Methods and code for 'classical' age-modelling of radiocarbon sequences. Quat. Geochronol. 5, 512–518. https://doi.org/10.1016/j.quageo.2010.01.002

Boës, X., Rydberg, J., Martinez-Cortizas, A., Bindler, R., Renberg, I., 2011. Evaluation of conservative lithogenic elements (Ti, Zr, Al, and Rb) to study anthropogenic element enrichments in lake sediments. J. Paleolimnol. 46, 75–87. https://doi.org/10.1007/s10933-011-9515-z

Brisset, E., Guiter, F., Miramont, C., Revel, M., Anthony, E.J., Delhon, C., Arnaud, F., Malet, E., de Beaulieu, J.-L., 2015. Lateglacial/Holocene environmental changes in the Mediterranean Alps inferred from lacustrine sediments. Quat. Sci. Rev. 110, 49–71. https://doi.org/10.1016/j.quascirev.2014.12.004

Brisset, E., Guiter, F., Miramont, C., Troussier, T., Sabatier, P., Poher, Y., Cartier, R., Arnaud, F., Malet, E., Anthony, E.J., 2017. The overlooked human influence in historic and prehistoric floods in the European Alps. Geology 45, 347–350. https://doi.org/10.1130/G38498.1

Brisset, E., Miramont, C., Guiter, F., Anthony, E.J., Tachikawa, K., Poulenard, J., Arnaud, F., Delhon, C., Meunier, J.-D., Bard, E., Suméra, F., 2013. Non-reversible geosystem destabilisation at 4200 cal. BP: Sedimentological, geochemical and botanical markers of soil erosion recorded in a Mediterranean alpine lake. The Holocene 23, 1863–1874. https://doi.org/10.1177/0959683613508158

Brisset, E., Miramont, C., Guiter, F., Arnaud, F., Anthony, E., Delhon, C., Guibal, F., Cartier, R., Poher, Y., Chaumillon, E., 2014. A new contribution to the chronology of the deglaciation in the Upper Verdon Valley (Lake Allos, Southern French Alps). Quaternaire 25. https://doi.org/10.4000/quaternaire.7028

Brüske, A., Weyer, S., Zhao, M.-Y., Planavsky, N.J., Wegwerth, A., Neubert, N., Dellwig, O., Lau, K.V., Lyons, T.W., 2020. Correlated molybdenum and uranium isotope signatures in modern anoxic sediments: Implications for their use as paleo-redox proxy. Geochim. Cosmochim. Acta 270, 449–474. https://doi.org/10.1016/j.gca.2019.11.031

Chabaux, F., Riotte, J., Dequincey, O., 2003. U-Th-Ra Fractionation During Weathering and River Transport. Rev. Mineral. Geochem. 52, 533–576. https://doi.org/10.2113/0520533

Chappaz, A., Gobeil, C., Tessier, A., 2010. Controls on uranium distribution in lake sediments. Geochim. Cosmochim. Acta 74, 203–214. https://doi.org/10.1016/j.gca.2009.09.026

Chase, Z., Anderson, R.F., Fleisher, M.Q., 2001. Evidence from authigenic uranium for increased productivity of the glacial subantarctic ocean. Paleoceanography 16, 468–478. https://doi.org/10.1029/2000PA000542

Chawchai, S., Kylander, M.E., Chabangborn, A., Löwemark, L., Wohlfarth, B., 2016. Testing commonly used X-ray fluorescence core scanning-based proxies for organic-rich lake sediments and peat. Boreas 45, 180–189. https://doi.org/10.1111/bor.12145

Cumberland, S.A., Douglas, G., Grice, K., Moreau, J.W., 2016. Uranium mobility in organic matter-rich sediments: A review of geological and geochemical processes. Earth-Sci. Rev. 159, 160–185. https://doi.org/10.1016/j.earscirev.2016.05.010

Dang, D.H., Wang, W., Pelletier, P., Poulain, A.J., Evans, R.D., 2018. Uranium dispersion from U tailings and mechanisms leading to U accumulation in sediments: Insights from biogeochemical and isotopic approaches. Sci. Total Environ. 610–611, 880–891. https://doi.org/10.1016/j.scitotenv.2017.08.156

Edgington, D.N., Robbins, J.A., Colman, S.M., Orlandini, K.A., Gustin, M.-P., 1996. Uranium-series disequilibrium, sedimentation, diatom frustules, and paleoclimate change in Lake Baikal. Earth Planet. Sci. Lett. 142, 29–42. https://doi.org/10.1016/0012-821X(96)00085-4

Elbaz-Poulichet, F., Guédron, S., Anne-Lise, D., Freydier, R., Perrot, V., Rossi, M., Piot, C., Delpoux, S., Sabatier, P., 2020. A 10,000-year record of trace metal and metalloid (Cu, Hg, Sb, Pb)

deposition in a western Alpine lake (Lake Robert, France): Deciphering local and regional mining contamination. Quat. Sci. Rev. 228, 106076. https://doi.org/10.1016/j.quascirev.2019.106076

Fisher, N.S., Teyssié, J.-L., Krishnaswami, S., Baskaran, M., 1987. Accumulation of Th, Pb, U, and Ra in marine phytoplankton and its geochemical significance1. Limnol. Oceanogr. 32, 131–142. https://doi.org/10.4319/lo.1987.32.1.0131

Giguet-Covex, C., Arnaud, F., Poulenard, J., Disnar, J.-R., Delhon, C., Francus, P., David, F., Enters, D., Rey, P.-J., Delannoy, J.-J., 2011. Changes in erosion patterns during the Holocene in a currently treeless subalpine catchment inferred from lake sediment geochemistry (Lake Anterne, 2063 m a.s.l., NW French Alps): The role of climate and human activities: The Holocene. https://doi.org/10.1177/0959683610391320

Giguet-Covex, C., Pansu, J., Arnaud, F., Rey, P.-J., Griggo, C., Gielly, L., Domaizon, I., Coissac, E., David, F., Choler, P., Poulenard, J., Taberlet, P., 2014. Long livestock farming history and human landscape shaping revealed by lake sediment DNA. Nat. Commun. 5, 3211. https://doi.org/10.1038/ncomms4211

Gilfedder, B.S., Petri, M., Wessels, M., Biester, H., 2011. Bromine species fluxes from Lake Constance's catchment, and a preliminary lake mass balance. Geochim. Cosmochim. Acta 75, 3385–3401. https://doi.org/10.1016/j.gca.2011.03.021

Goldberg, E.L., Chebykin, E.P., Zhuchenko, N.A., S.S.Vorobyeva, Stepanova, O.G., Khlystov, O.M., Ivanov, E.V., Weinberg, E., Gvozdkov, A.N., 2010. Uranium isotopes as proxies of the environmental history of the Lake Baikal watershed (East Siberia) during the past 150ka. Palaeogeogr. Palaeoclimatol. Palaeoecol., Paleolimnology 294, 16–29. https://doi.org/10.1016/j.palaeo.2009.08.030

Gordon, E.S., Goñi, M.A., 2003. Sources and distribution of terrigenous organic matter delivered by the Atchafalaya River to sediments in the northern Gulf of Mexico. Geochim. Cosmochim. Acta 67, 2359–2375. https://doi.org/10.1016/S0016-7037(02)01412-6

Guevara, S.R., Rizzo, A., Daga, R., Williams, N., Villa, S., 2019. Bromine as indicator of source of lacustrine sedimentary organic matter in paleolimnological studies. Quat. Res. 92, 257–271. https://doi.org/10.1017/qua.2018.125

Heiri, O., Ilyashuk, B., Millet, L., Samartin, S., Lotter, A.F., 2015. Stacking of discontinuous regional palaeoclimate records: Chironomid-based summer temperatures from the Alpine region. The Holocene 25, 137–149. https://doi.org/10.1177/0959683614556382

Hinojosa, J.L., Stirling, C.H., Reid, M.R., Moy, C.M., Wilson, G.S., 2016. Trace metal cycling and 238U/235U in New Zealand's fjords: Implications for reconstructing global paleoredox conditions in organic-rich sediments. Geochim. Cosmochim. Acta 179, 89–109. https://doi.org/10.1016/j.gca.2016.02.006

IRMM, 2005. Certificate of analysis: Isotopic Reference Material IRMM-184. Institute for Reference Materials and Measurements, Geel (Belgium).

Kalin, M., Wheeler, W.N., Meinrath, G., 2005. The removal of uranium from mining waste water using algal/microbial biomass. J. Environ. Radioact. 78, 151–177. https://doi.org/10.1016/j.jenvrad.2004.05.002

Kerfoot, W.C., Robbins, J.A., Weider, L.J., 1999. A new approach to historical reconstruction: Combining descriptive and experimental paleolimnology. Limnol. Oceanogr. 44, 1232–1247. https://doi.org/10.4319/lo.1999.44.5.1232

Landais, P., 1996. Organic geochemistry of sedimentary uranium ore deposits. Ore Geol. Rev., Organics and Ore Deposits 11, 33–51. https://doi.org/10.1016/0169-1368(95)00014-3

Langmuir, D., 1978. Uranium solution-mineral equilibria at low temperatures with applications to sedimentary ore deposits. Geochim. Cosmochim. Acta 42, 547–569. https://doi.org/10.1016/0016-7037(78)90001-7

Lau, K.V., Romaniello, S.J., Zhang, F., 2019. The Uranium Isotope Paleoredox Proxy, Elements in Geochemical Tracers in Earth System Science. Cambridge University Press. https://doi.org/10.1017/9781108584142

Le Roy, M., Deline, P., Carcaillet, J., Schimmelpfennig, I., Ermini, M., 2017. 10Be exposure dating of the timing of Neoglacial glacier advances in the Ecrins-Pelvoux massif, southern French Alps. Quat. Sci. Rev. 178, 118–138. https://doi.org/10.1016/j.quascirev.2017.10.010

Le Roy, M., Nicolussi, K., Deline, P., Astrade, L., Edouard, J.-L., Miramont, C., Arnaud, F., 2015. Calendar-dated glacier variations in the western European Alps during the Neoglacial: the Mer de Glace record, Mont Blanc massif. Quat. Sci. Rev. 108, 1–22. https://doi.org/10.1016/j.quascirev.2014.10.033

Lefebvre, P., Gourgiotis, A., Mangeret, A., Sabatier, P., Le Pape, P., Diez, O., Louvat, P., Menguy, N., Merrot, P., Baya, C., Zebracki, M., Blanchart, P., Malet, E., Jézéquel, D., Reyss, J.-L., Bargar, J.R., Gaillardet, J., Cazala, C., Morin, G., 2021. Diagenetic formation of uranium-silica polymers in lake sediments over 3,300 years. Proc. Natl. Acad. Sci. 118. https://doi.org/10.1073/pnas.2021844118

Leri, A.C., Hakala, J.A., Marcus, M.A., Lanzirotti, A., Reddy, C.M., Myneni, S.C.B., 2010. Natural organobromine in marine sediments: New evidence of biogeochemical Br cycling. Glob. Biogeochem. Cycles 24. https://doi.org/10.1029/2010GB003794

Leri, A.C., Myneni, S.C.B., 2012. Natural organobromine in terrestrial ecosystems. Geochim. Cosmochim. Acta 77, 1–10. https://doi.org/10.1016/j.gca.2011.11.012

Liu, X., Colman, S.M., Brown, E.T., Minor, E.C., Li, H., 2013. Estimation of carbonate, total organic carbon, and biogenic silica content by FTIR and XRF techniques in lacustrine sediments. J. Paleolimnol. 50, 387–398.

Magny, M., Combourieu-Nebout, N., de Beaulieu, J.L., Bout-Roumazeilles, V., Colombaroli, D., Desprat, S., Francke, A., Joannin, S., Ortu, E., Peyron, O., Revel, M., Sadori, L., Siani, G., Sicre, M.A., Samartin, S., Simonneau, A., Tinner, W., Vannière, B., Wagner, B., Zanchetta, G., Anselmetti, F., Brugiapaglia, E., Chapron, E., Debret, M., Desmet, M., Didier, J., Essallami, L., Galop, D., Gilli, A., Haas, J.N., Kallel, N., Millet, L., Stock, A., Turon, J.L., Wirth, S., 2013. North-south palaeohydrological contrasts in the central Mediterranean during the Holocene: tentative synthesis and working hypotheses. Clim. Past 9, 2043–2071. https://doi.org/10.5194/cp-9-2043-2013

Maher, K., Bargar, J.R., Brown, G.E., 2013. Environmental Speciation of Actinides. Inorg. Chem. 52, 3510–3532. https://doi.org/10.1021/ic301686d

Mangeret, A., Blanchart, P., Alcalde, G., Amet, X., Cazala, C., Gallerand, M.-O., 2018. An evidence of chemically and physically mediated migration of 238U and its daughter isotopes in the vicinity of a former uranium mine. J. Environ. Radioact. 195, 67–71. https://doi.org/10.1016/j.jenvrad.2018.08.018

Mann, H., Fyfe, W.S., 1985. Uranium uptake by algae: experimental and natural environments. Can. J. Earth Sci. 22, 1899–1903. https://doi.org/10.1139/e85-205

Mann, H., Fyfe, W.S., 1984. An experimental study of algal uptake of U, Ba, V, Co and Ni from dilute solutions. Chem. Geol. 44, 385–398. https://doi.org/10.1016/0009-2541(84)90150-5

Marsicek, J., Shuman, B.N., Bartlein, P.J., Shafer, S.L., Brewer, S., 2018. Reconciling divergent trends and millennial variations in Holocene temperatures. Nature 554, 92–96. https://doi.org/10.1038/nature25464

Martin-Puertas, C., Brauer, A., Dulski, P., Brademann, B., 2012. Testing climate–proxy stationarity throughout the Holocene: an example from the varved sediments of Lake Meerfelder Maar (Germany). Quat. Sci. Rev. 58, 56–65. https://doi.org/10.1016/j.quascirev.2012.10.023

Martrat, B., Jimenez-Amat, P., Zahn, R., Grimalt, J.O., 2014. Similarities and dissimilarities between the last two deglaciations and interglaciations in the North Atlantic region. Quat. Sci. Rev. 99, 122–134. https://doi.org/10.1016/j.quascirev.2014.06.016

Mayer, L.M., Macko, S.A., Mook, W.H., Murray, S., 1981. The distribution of bromine in coastal sediments and its use as a source indicator for organic matter. Org. Geochem. 3, 37–42. https://doi.org/10.1016/0146-6380(81)90011-5

Mayer, L.M., Schick, L.L., Allison, M.A., Ruttenberg, K.C., Bentley, S.J., 2007. Marine vs. terrigenous organic matter in Louisiana coastal sediments: The uses of bromine:organic carbon ratios. Mar. Chem. 107, 244–254. https://doi.org/10.1016/j.marchem.2007.07.007

McManus, J., Berelson, W.M., Klinkhammer, G.P., Hammond, D.E., Holm, C., 2005. Authigenic uranium: Relationship to oxygen penetration depth and organic carbon rain. Geochim. Cosmochim. Acta 69, 95–108. https://doi.org/10.1016/j.gca.2004.06.023

Meyers, P.A., Teranes, J.L., 2001. Sediment Organic Matter, in: Last, W.M., Smol, J.P. (Eds.), Tracking Environmental Change Using Lake Sediments: Physical and Geochemical Methods, Developments in Paleoenvironmental Research. Springer Netherlands, Dordrecht, pp. 239–269. https://doi.org/10.1007/0-306-47670-3_9

Missiaen, L., Pichat, S., Waelbroeck, C., Douville, E., Bordier, L., Dapoigny, A., Thil, F., Foliot, L., Wacker, L., 2018. Downcore Variations of Sedimentary Detrital (238U/232Th) Ratio: Implications on the Use of 230Thxs and 231Paxs to Reconstruct Sediment Flux and Ocean Circulation. Geochem. Geophys. Geosystems 19, 2560–2573. https://doi.org/10.1029/2017GC007410

Mourier, B., Poulenard, J., Carcaillet, C., Williamson, D., 2010. Soil evolution and subalpine ecosystem changes in the French Alps inferred from geochemical analysis of lacustrine sediments. J. Paleolimnol. 44, 571–587. https://doi.org/10.1007/s10933-010-9438-0

Naeher, S., Gilli, A., North, R.P., Hamann, Y., Schubert, C.J., 2013. Tracing bottom water oxygenation with sedimentary Mn/Fe ratios in Lake Zurich, Switzerland. Chem. Geol. 352, 125–133. https://doi.org/10.1016/j.chemgeo.2013.06.006

NBL, 2010. Certificate of analysis: Uranyl Nitrate Assay and Isotopic Solution CRM 145. New Brunswick Laboratory, U.S. Department of Energy, Argonne, IL (USA).

Nuttin, L., Francus, P., Preda, M., Ghaleb, B., Hillaire-Marcel, C., 2013. Authigenic, detrital and diagenetic minerals in the Laguna Potrok Aike sediment sequence. Quat. Sci. Rev., Potrok Aike Maar Lake Sediment Archive Drilling Project (PASADO) 71, 109–118. https://doi.org/10.1016/j.quascirev.2012.09.027

Och, L.M., Müller, B., März, C., Wichser, A., Vologina, E.G., Sturm, M., 2016. Elevated uranium concentrations in Lake Baikal sediments: Burial and early diagenesis. Chem. Geol. 441, 92–105. https://doi.org/10.1016/j.chemgeo.2016.08.001

Owen, D.E., Otton, J.K., 1995. Mountain wetlands: Efficient uranium filters — potential impacts. Ecol. Eng., The role of vegetation in created and restored wetlands 5, 77–93. https://doi.org/10.1016/0925-8574(95)00013-9

Peña, J., Straub, M., Flury, V., Loup, E., Corcho, J., Steinmann, P., Bochud, F., Froidevaux, P., 2020. Origin and stability of uranium accumulation-layers in an Alpine histosol. Sci. Total Environ. 727, 138368. https://doi.org/10.1016/j.scitotenv.2020.138368

Perrier, G., 1980. La structure des Alpes occidentales déduite des données géophysiques. Eclogae Geol. Helvetiae 7, 407–424. https://doi.org/doi.org/10.5169/seals-164963

Phedorin, M.A., Goldberg, E.L., 2005. Prediction of absolute concentrations of elements from SR XRF scan measurements of natural wet sediments. Nucl. Instrum. Methods Phys. Res. Sect. Accel. Spectrometers Detect. Assoc. Equip., Proceedings of the XV International Synchrotron Radiation Conference 543, 274–279. https://doi.org/10.1016/j.nima.2005.01.240

Phedorin, M.A., Goldberg, E.L., Grachev, M.A., Levina, O.L., Khlystov, O.M., Dolbnya, I.P., 2000. The comparison of biogenic silica, Br and Nd distributions in the sediments of Lake Baikal as proxies of changing paleoclimates of the last 480kyr. Nucl. Instrum. Methods Phys. Res. Sect. Accel. Spectrometers Detect. Assoc. Equip. 448, 400–406. https://doi.org/10.1016/S0168-9002(99)00726-3

Poulenard, J., 2011. Des empreintes pédologiques dans les bassins versants et les archives naturelles. (thesis). Université de Savoie.

Pyankov, V.I., Ziegler, H., Akhani, H., Deigele, C., Lüttge, U., 2010. European plants with C4 photosynthesis: geographical and taxonomic distribution and relations to climate

parameters. Bot. J. Linn. Soc. 163, 283–304. https://doi.org/10.1111/j.1095-8339.2010.01062.x

R Core Team, 2019. R: A language and environment for statistical computing. R Foundation for Statistical Computing, Vienna (Austria).

Regenspurg, S., Margot-Roquier, C., Harfouche, M., Froidevaux, P., Steinmann, P., Junier, P., Bernier-Latmani, R., 2010. Speciation of naturally-accumulated uranium in an organic-rich soil of an alpine region (Switzerland). Geochim. Cosmochim. Acta 74, 2082–2098. https://doi.org/10.1016/j.gca.2010.01.007

Reimer, P.J., Austin, W.E.N., Bard, E., Bayliss, A., Blackwell, P.G., Ramsey, C.B., Butzin, M., Cheng, H., Edwards, R.L., Friedrich, M., Grootes, P.M., Guilderson, T.P., Hajdas, I., Heaton, T.J., Hogg, A.G., Hughen, K.A., Kromer, B., Manning, S.W., Muscheler, R., Palmer, J.G., Pearson, C., Plicht, J. van der, Reimer, R.W., Richards, D.A., Scott, E.M., Southon, J.R., Turney, C.S.M., Wacker, L., Adolphi, F., Büntgen, U., Capano, M., Fahrni, S.M., Fogtmann-Schulz, A., Friedrich, R., Köhler, P., Kudsk, S., Miyake, F., Olsen, J., Reinig, F., Sakamoto, M., Sookdeo, A., Talamo, S., 2020. The IntCal20 Northern Hemisphere Radiocarbon Age Calibration Curve (0–55 cal kBP). Radiocarbon 62, 725–757. https://doi.org/10.1017/RDC.2020.41

Renberg, I., Bindler, R., Brännvall, M.-L., 2001. Using the historical atmospheric lead-deposition record as a chronological marker in sediment deposits in Europe. The Holocene 11, 511–516. https://doi.org/10.1191/095968301680223468

Reyss, J.-L., Schmidt, S., Legeleux, F., Bonté, P., 1995. Large, low background well-type detectors for measurements of environmental radioactivity. Nucl. Instrum. Methods Phys. Res. Sect. Accel. Spectrometers Detect. Assoc. Equip. 357, 391–397. https://doi.org/10.1016/0168-9002(95)00021-6

Sabatier, P., Wilhelm, B., Ficetola, G.F., Moiroux, F., Poulenard, J., Develle, A.-L., Bichet, A., Chen, W., Pignol, C., Reyss, J.-L., Gielly, L., Bajard, M., Perrette, Y., Malet, E., Taberlet, P., Arnaud, F., 2017. 6-kyr record of flood frequency and intensity in the western Mediterranean Alps – Interplay of solar and temperature forcing. Quat. Sci. Rev. 170, 121–135. https://doi.org/10.1016/j.quascirev.2017.06.019

Sáez, A., Valero-Garcés, B.L., Giralt, S., Moreno, A., Bao, R., Pueyo, J.J., Hernández, A., Casas, D., 2009. Glacial to Holocene climate changes in the SE Pacific. The Raraku Lake sedimentary record (Easter Island, 27°S). Quat. Sci. Rev. 28, 2743–2759. https://doi.org/10.1016/j.quascirev.2009.06.018

Samartin, S., Heiri, O., Joos, F., Renssen, H., Franke, J., Brönnimann, S., Tinner, W., 2017. Warm Mediterranean mid-Holocene summers inferred from fossil midge assemblages. Nat. Geosci. 10, 207–212. https://doi.org/10.1038/ngeo2891

Seeber, J., Seeber, G.U.H., 2005. Effects of land-use changes on humus forms on alpine pastureland (Central Alps, Tyrol). Geoderma 124, 215–222. https://doi.org/10.1016/j.geoderma.2004.05.002

Spirakis, C.S., 1996. The roles of organic matter in the formation of uranium deposits in sedimentary rocks. Ore Geol. Rev., Organics and Ore Deposits 11, 53–69. https://doi.org/10.1016/0169-1368(95)00015-1

Stetten, L., Mangeret, A., Brest, J., Seder-Colomina, M., Le Pape, P., Ikogou, M., Zeyen, N., Thouvenot, A., Julien, A., Alcalde, G., Reyss, J.L., Bombled, B., Rabouille, C., Olivi, L., Proux, O., Cazala, C., Morin, G., 2018. Geochemical control on the reduction of U(VI) to mononuclear U(IV) species in lacustrine sediments. Geochim. Cosmochim. Acta 222, 171–186. https://doi.org/10.1016/j.gca.2017.10.026

Talon, B., 2010. Reconstruction of Holocene high-altitude vegetation cover in the French southern Alps: evidence from soil charcoal. The Holocene 20, 35–44. https://doi.org/10.1177/0959683609348842

Thevenon, F., Adatte, T., Spangenberg, J.E., Anselmetti, F.S., 2012. Elemental (C/N ratios) and isotopic (δ15Norg, δ13Corg) compositions of sedimentary organic matter from a high-altitude mountain lake (Meidsee, 2661 m a.s.l., Switzerland): Implications for Lateglacial and

Holocene Alpine landscape evolution. The Holocene 22, 1135–1142. https://doi.org/10.1177/0959683612441841

Tribovillard, N., Algeo, T.J., Lyons, T., Riboulleau, A., 2006. Trace metals as paleoredox and paleoproductivity proxies: An update. Chem. Geol. 232, 12–32. https://doi.org/10.1016/j.chemgeo.2006.02.012

Vanniere, B., Magny, M., Joannin, S., Simonneau, A., Wirth, S., Hamman, Y., Chapron, E., Gilli, A., Desmet, M., Anselmetti, F., 2013. Orbital changes, variation in solar activity and increased anthropogenic activities: controls on the Holocene flood frequency in the Lake Ledro area, Northern Italy. Clim. Past 9, 1193–1209. https://doi.org/10.5194/cp-9-1193-2013

Walsh, K., Mocci, F., Palet-Martinez, J., 2007. Nine thousand years of human/landscape dynamics in a high altitude zone in the southern French Alps (Parc National des Ecrins, Hautes-Alpes). Preistoria Alp. 42, 9–22.

Wang, W., Dang, D.H., Novotnik, B., Phan, T.T., Evans, R.D., 2019. Variations in U concentrations and isotope signatures in two Canadian lakes impacted by U mining: A combination of anthropogenic and biogeochemical processes. Chem. Geol. 506, 58–67. https://doi.org/10.1016/j.chemgeo.2018.12.029

Wang, Y., Frutschi, M., Suvorova, E., Phrommavanh, V., Descostes, M., Osman, A.A.A., Geipel, G., Bernier-Latmani, R., 2013. Mobile uranium(IV)-bearing colloids in a mining-impacted wetland. Nat. Commun. 4, 1–9. https://doi.org/10.1038/ncomms3942

Weltje, G.J., Tjallingii, R., 2008. Calibration of XRF core scanners for quantitative geochemical logging of sediment cores: Theory and application. Earth Planet. Sci. Lett. 274, 423–438. https://doi.org/10.1016/j.epsl.2008.07.054

Whitlock, C., Dean, W.E., Fritz, S.C., Stevens, L.R., Stone, J.R., Power, M.J., Rosenbaum, J.R., Pierce, K.L., Bracht-Flyr, B.B., 2012. Holocene seasonal variability inferred from multiple proxy records from Crevice Lake, Yellowstone National Park, USA. Palaeogeogr. Palaeoclimatol. Palaeoecol. 331–332, 90–103. https://doi.org/10.1016/j.palaeo.2012.03.001

Wilhelm, B., Arnaud, F., Sabatier, P., Crouzet, C., Brisset, E., Chaumillon, E., Disnar, J.-R., Guiter, F., Malet, E., Reyss, J.-L., Tachikawa, K., Bard, E., Delannoy, J.-J., 2012. 1400 years of extreme precipitation patterns over the Mediterranean French Alps and possible forcing mechanisms. Quat. Res. 78, 1–12. https://doi.org/10.1016/j.yqres.2012.03.003

Wilhelm, B., Arnaud, F., Sabatier, P., Magand, O., Chapron, E., Courp, T., Tachikawa, K., Fanget, B., Malet, E., Pignol, C., Bard, E., Delannoy, J.J., 2013. Palaeoflood activity and climate change over the last 1400 years recorded by lake sediments in the north-west European Alps. J. Quat. Sci. 28, 189–199. https://doi.org/10.1002/jqs.2609

Wirth, S.B., Glur, L., Gilli, A., Anselmetti, F.S., 2013. Holocene flood frequency across the Central Alps – solar forcing and evidence for variations in North Atlantic atmospheric circulation. Quat. Sci. Rev. 80, 112–128. https://doi.org/10.1016/j.quascirev.2013.09.002

Woodward, C.A., Gadd, P.S., 2019. The potential power and pitfalls of using the X-ray fluorescence molybdenum incoherent: Coherent scattering ratio as a proxy for sediment organic content. Quat. Int., Advances in Data Quantification and Application of high resolution XRF Core Scanners 514, 30–43. https://doi.org/10.1016/j.quaint.2018.11.031

Yang, Y., Fang, X., Li, M., Galy, A., Koutsodendris, A., Zhang, W., 2015. Paleoenvironmental implications of uranium concentrations in lacustrine calcareous clastic-evaporite deposits in the western Qaidam Basin. Palaeogeogr. Palaeoclimatol. Palaeoecol. 417, 422–431. https://doi.org/10.1016/j.palaeo.2014.10.002

Yu, E.-F., Liang, C.-H., Chen, M.-T., 1999. Authigenic uranium in marine sediments of the Benguela Current upwelling region during the last glacial period. Terr. Atmospheric Ocean. Sci. 10, 201–214.

Zheng, Y., Anderson, R.F., van Geen, A., Fleisher, M.Q., 2002. Remobilization of authigenic uranium in marine sediments by bioturbation. Geochim. Cosmochim. Acta 66, 1759–1772. https://doi.org/10.1016/S0016-7037(01)00886-9

Ziegler, M., Jilbert, T., Lange, G.J. de, Lourens, L.J., Reichart, G.-J., 2008. Bromine counts from XRF scanning as an estimate of the marine organic carbon content of sediment cores. Geochem. Geophys. Geosystems 9. https://doi.org/10.1029/2007GC001932